Astrophysical Neutrino Telescopes

A. B. McDonald
SNO Institute, Queen's University, Kingston, Canada K7L 3N6

C. Spiering
DESY Zeuthen, Platanenallee 6, D-15738 Zeuthen, Germany

S. Schönert
Max-Planck-Institut für Kernphysik, Saupfercheckweg 1, 69117 Heidelberg, Germany

E. T. Kearns
Boston Univ., Dept. of Physics, 590 Commonwealth Ave., Boston, MA 02215 USA

T. Kajita
Institute for Cosmic Ray Research, Univ. of Tokyo, Kashiwa-no-ha 5-1-5, Kashiwa, Chiba 277-8582, Japan

(Dated: November 17, 2003)

This review describes telescopes designed to study neutrinos from astrophysical sources. These sources include the Sun and Supernovae emitting neutrino energies up to tens of MeV, atmospheric neutrino sources caused by cosmic ray interactions and other sources generating neutrino energies ranging up to 1×10^{20} eV. Measurements with these telescopes also provide information on neutrino properties including clear evidence for neutrino flavor change. Telescopes in operation in the past and present are described, along with plans for future instruments to expand this rapidly growing field of particle astrophysics.

PACS numbers: 95.55.Vj, 95.85.Ry, 96.60.Vg, 14.60.Pq

I. INTRODUCTION

A new generation of astronomical instruments has evolved, starting with the radiochemical solar neutrino detector of Ray Davis and his collaborators [1] more than 30 years ago. This generation of instruments is part of the developing field of particle astrophysics, where particles from astrophysical objects are used to provide information about those objects and about the properties of the particles themselves. Since astrophysical objects can provide intensities and energies far outstripping any terrestrial source, this area of study has become a significant one for the field of particle physics. Neutrinos have a number of favorable properties that make them attractive as a means to study astrophysical objects, so neutrino telescopes have significant value for astrophysics as well.

Neutrinos have no electric charge and are not sensitive to the strong interaction. Their mass and magnetic moments are very small and so they undergo very few interactions even in the densest matter. This makes them ideal candidates for the study of otherwise inaccessible astrophysical regions, such as the center of the Sun, or distant astrophysical sources without distortion of their trajectories by intergalactic magnetic fields or material. Neutrinos are known to have three active species (electron, muon, tau) associated with these three lepton generations. Experiments on the decay properties of the Z Weak Boson [2] have shown that there are three (2.981 $\pm$ 0.008) such active species.

The energies of neutrinos detected by the telescopes described in this article include: from a few 100 keV to 30 MeV for solar and supernova neutrinos; 0.1 GeV to a few TeV for neutrinos generated by cosmic rays interacting with the atmosphere; and much higher energies, ranging up to 1×10^{20} eV for the highest energy neutrino sources. The detection techniques differ substantially, but all detectors are situated in locations where interfering backgrounds are shielded to a substantial degree because the experiments tend to have very low neutrino detection rates as a result of the small interaction probability. The experiments seeking neutrinos below about 1000 GeV are typically in underground locations to range out cosmic ray background and the highest energy experiments are typically under ice or under water in order to combine effective shielding with very large detection volumes.

The sections of the paper include: 2. Solar Neutrino Detectors; 3. Supernova Neutrino Detectors; 4. Atmospheric Neutrino Detectors; 5. Very High Energy Neutrino Detectors. This subdivision of detector groups is somewhat arbitrary since there is substantial overlap in the capabilities of the detectors, and all of them have some degree of sensitivity for supernova neutrino detection. However, this choice has some advantages for description, as the detectors are described in the section covering the primary scientific motivation for the detector and reference to additional capabilities may be mentioned further in another section. This paper is mainly intended to describe the principal features of the detec-

tors themselves, but in each case the physics motivation for the detectors is presented, along with the detector scientific capability and a succinct summary of the results obtained to date or anticipated for the future.

There are many astrophysical motivations for the detection of neutrinos with neutrino telescopes, as well as opportunities to determine particle physics properties of neutrinos themselves through the use of astrophysical sources. The complementary nature of this information has made neutrino telescopes a central part of the rapidly developing field of Particle Astrophysics.

Some of the principal astrophysical motivations are as follows. The neutrinos produced in the Sun arise from the principal nuclear reactions powering the Sun. Detailed models of the Sun have been developed that match other measured solar properties very well and predict a spectrum of neutrinos from a number of the nuclear reactions. The study of neutrinos from the Sun over the full range of energies provides a very detailed test of solar models, including otherwise inaccessible information from the core region.

Atmospheric neutrinos arise primarily from the decay of muons, pions or kaons produced by energetic cosmic rays interacting with the atmosphere. Measurements of neutrino fluxes over a broad range of energies can be combined with other sources of information to obtain an understanding of cosmic rays from astrophysical sources. The highest energy neutrinos arise from high energy cosmic rays, protons or nuclei. One of the objectives of neutrino detection is to determine the origins and acceleration mechanisms of these very high energy charged particles. Neutrinos from Supernovae include electron neutrinos arising from the conversion of neutrons to protons during the initial infall as well as electron, mu and tau neutrinos and anti-neutrinos produced during the expansion phase following the point of maximum compression. Neutrinos carry away the majority of the energy from a supernova and can provide very detailed information on the processes involved in these spectacular astronomical events.

Neutrinos from astrophysical sources can also be used to study detailed properties of neutrinos and results from these measurements have provided very valuable information, including the first clear indications of neutrino flavor change (i.e. the change of a neutrino of one family into one of another family) and information on neutrino mass differences. Some of the particle physics information that has been obtained from astrophysical neutrinos is as follows.

In the case of neutrino mixing, the neutrino flavor fields ν_ℓ are superpositions of the components ν_k of the fields of neutrinos with definite masses m_k:

$$\nu_\ell = \sum_{k=1}^{3} U_{\ell k}\, \nu_k \qquad (\ell = e, \mu, \tau)\,, \tag{1}$$

where U is the 3 x 3 unitary Maki-Nakagawa-Sakata-Pontecorvo (MNSP) mixing matrix [3].

When the neutrinos travel in a vacuum or low density region, the linear combinations are changed so that the detected neutrino types appear to oscillate among the neutrino flavors. If the masses are not strongly degenerate, then the 3 x 3 MNSP matrix can be separated into 2 x 2 matrices affecting oscillation among two masses almost independently of the third. In this case there is one Δm^2 such as $m_2^2 - m_1^2$ for the masses involved and the mixing matrix

$$U = \begin{pmatrix} \cos\theta & \sin\theta \\ -\sin\theta & \cos\theta \end{pmatrix} \tag{2}$$

For this simplest case where two mass eigenstates dominate the process, the following probability is predicted for subsequent detection of a given neutrino type after it has traveled for a distance L in vacuum:

$$P = 1 - sin^2(2\theta) sin^2(1.27\Delta m^2 L/E)$$

where Δm^2 is in eV^2, L is the source-detector distance in meters, E is the neutrino energy in MeV and θ is a mixing angle. In order for a significant fraction of neutrinos to change their flavor, $sin^2(2\theta)$ must be reasonably large and $\Delta m^2 L/E$ must be appropriate for the source and detector involved. This process has been used to interpret atmospheric neutrino data observed by the Super-Kamiokande detector as described in Section 4 wherein muon neutrinos appear to oscillate predominantly to tau neutrinos as they traverse the Earth. These measurements can be used to define elements of the MNSP matrix, in particular, Δm^2_{23} and $sin^2\theta_{23}$.

Additional effects can occur when neutrinos pass through regions of dense matter. These effects are associated with the fact that electron neutrinos can have interactions with electrons through W exchange in addition to the Z exchange occurring for all flavors. These effects can result in matter enhancement of the oscillation process [4], the so-called MSW (Mikheyev-Smirnov-Wolfenstein) effect. This enhancement greatly broadens the region of Δm^2_{12} and $sin^2\theta_{12}$ where significant effects can occur and introduces an additional dependence on the neutrino energy.

The Sudbury Neutrino Observatory (SNO) has provided evidence [5] for neutrino flavor change by observing clear differences between one reaction sensitive to only electron neutrinos and another sensitive equally to all neutrino types. The results show that about 2/3 of the electron neutrinos produced in the Sun appear to have transformed to other types before detection on Earth. A similar conclusion is reached by comparing the SNO results with the measurements of solar neutrinos by Super-Kamiokande [6], using a reaction with a small sensitivity to other neutrino types in addition to electron neutrinos. These results, together with a number of other measurements of solar neutrinos with different energy thresholds, can be interpreted in terms of neutrino oscillations, providing additional information about elements of the MNSP matrix, particularly Δm^2_{12} and $sin^2\theta_{12}$.

Many other particle physics properties of neutrinos can be defined by measurements with neutrino telescopes, including limits on neutrino decay lifetimes and magnetic moments. Future experiments will also improve significantly on present neutrino mass and mixing parameters, particularly when combined with measurements from terrestrial sources such as reactors and accelerators.

The improved definition of neutrino properties through these measurements from astrophysical sources can, in turn, be used to improve our astrophysical information. For example, with the oscillation properties of neutrinos defined, it is possible to understand the original fluxes of solar electron neutrinos as a function of energy. This provides a very accurate test of solar models and adds to our understanding of the astrophysics of the Sun.

II. SOLAR NEUTRINOS

A. Physics and Astrophysics Motivations

1. *Astrophysics Motivations*

Solar models have been developed to a high level of sophistication [7, 8] and are capable of correct predictions for many of the measurable solar properties, including recent helioseismological results that probe the inner regions with unprecedented accuracy. The detection of neutrinos from the Sun provides information on the nuclear reactions and associated neutrino fluxes that pin down the properties of the solar core region with considerable accuracy. Neutrino fluxes have a strong dependence on the temperature of the core region and on other processes such as mixing of materials between various solar regions. Models of the Sun following standard assumptions [7, 8] are found to be remarkably successful for all properties other than neutrino fluxes. However, initial neutrino measurements either solely or primarily sensitive to electron neutrinos were found to be lower than expected because of the presence of neutrino flavor-changing processes. The possibility of a finite neutrino magnetic moment also enables solar magnetic fields to be probed with sensitivities restricted by current limits on the magnetic moments set by terrestrial or other astrophysical determinations.

The set of nuclear reactions thought to be primarily responsible for energy generation in the Sun are shown in Table 1 and fluxes predicted by a Standard Solar Model Calculation [7] assuming no neutrino flavor change are shown in Figure 1.

2. *Particle Physics Motivations*

As discussed above, the possibility to use copious quantities of neutrinos from the Sun to study the basic properties of neutrinos provides a further motivation for such measurements. The long baseline from the Sun to the Earth provides an opportunity for neutrinos to change their flavor through oscillation processes and the high density of electrons in the Sun can provide additional enhancement of such flavor change [4]. Limits on neutrino decay and on neutrino magnetic moments can also be obtained from such studies.

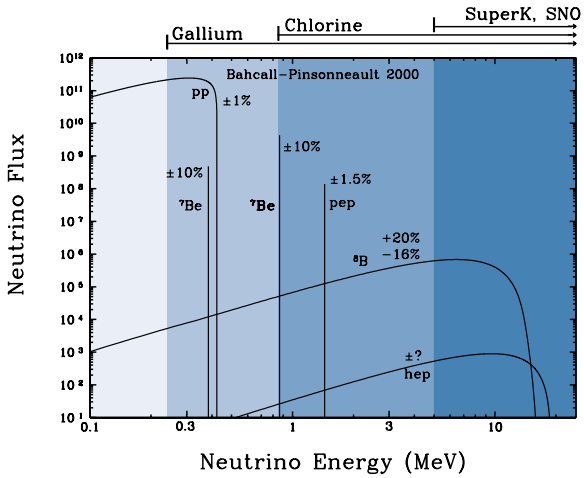

FIG. 1: Spectrum of neutrinos from the Sun as obtained by a Standard Solar Model calculation

B. Solar neutrino detection reactions

Solar neutrino detection reactions that have been used successfully to date fall into two main categories. 1. Radiochemical measurements involve the transformation of atoms of an element such as Cl or Ga into another radioactive element through inverse beta decay induced by electron neutrinos. These reactions can be observed by sweeping the radioactive elements from the detector volume and observing the subsequent decay. The measurements typically involve collection periods on the order of a month and subsequent decay measurement periods of many months. 2. Real-Time measurements involve the observation of events produced by neutrino interactions in the detector medium in real time. Experiments to date have used light and heavy water as media for real-time neutrino detection. The reactions that have been used involve elastic scattering of neutrinos from electrons, the inverse beta decay reaction on deuterium producing energetic electrons and inelastic scattering on deuterium producing free neutrons.

1. *Cherenkov Detection Process*

The real time detection reactions (including the capture of the neutrons produced in the latter reaction) all result in energetic electrons being produced that are observed via the Cerenkov process. Charged particles trav-

TABLE I: Principal nuclear reactions producing neutrinos in the Sun [7]

Neutrino Source	Energy [MeV]	Flux at Earth [10^{10} cm^{-2} s^{-1}]	^{35}Cl Production [SNU]	^{71}Ga Production [SNU]
pp ($pp \rightarrow de^{+}\nu_e$)	< 0.42	6.0	—-	69.7
pep ($pe^{-}p \rightarrow d\nu_e$)	1.4	0.014	0.22	2.8
^{7}Be (^{7}Be e^{-} $\rightarrow^{7}$Li ν_e)	0.38, 0.86	0.48	1.2	34.2
^{8}B (^{8}B $\rightarrow^{8}$Be* e$^{+}\nu_e$)	< 15	0.00051	5.8	12.1
^{3}He p (^{3}He p $\rightarrow^{4}$He e^{+} ν_e)	< 18.77	9.310^{-7}	0.04	0.1
^{13}N	< 1.20	0.055	0.09	3.4
^{15}O	< 1.73	0.048	0.33	5.5
^{17}F	< 1.74	0.00056	0.0	0.1
Total		6.5	7.6	128

elling in a transparent medium at greater than the group velocity of light in that medium radiate Cherenkov light. These photons have a continuous spectral distribution and are emitted in a forward cone whose axis is the direction of the electron and whose opening angle (θ) is given by

$$cos\ \theta = (n\beta)^{-1}$$

where n is the index of refraction in the medium and β is the electron's speed relative to the speed of light. For light and heavy water θ equals about 41 degrees for relativistic electrons. The number of photons emitted by the electrons is approximately proportional to the track length (and hence energy) and is about 350 photons per cm in the typical spectral range for which photomultipliers are sensitive (about 300 to 600 nanometers). The electron track length is about 0.45 cm per MeV in water for kinetic energies between 5 and 15 MeV, thus about 1100 photons are produced by a 7 MeV electron.

C. Radiochemical Detectors

1. *Homestake Cl Experiment*

The first detector to report fluxes of neutrinos from the Sun was the pioneering experiment of Ray Davis and coworkers [1] using 680 tons of liquid perchlorethylene sited 1480 meters underground (4300 meters water equivalent) in the Homestake gold mine near Lead, South Dakota, USA. This experiment employs the electron neutrino capture reaction on ^{37}Cl, producing ^{37}Ar atoms in the liquid. The radioactive ^{37}Ar atoms (35-day half life) are swept from the containment tank by flushing with helium gas about every 100 days. The ^{37}Ar atoms are condensed into sensitive proportional counters with high efficiency and the resulting decays are observed for many half-lives of ^{37}Ar. Production rates of about 0.5 argon atoms per day are observed, about three times lower than predictions of the Standard Solar Models [7, 8].

The experimental apparatus is shown in Figure 2.

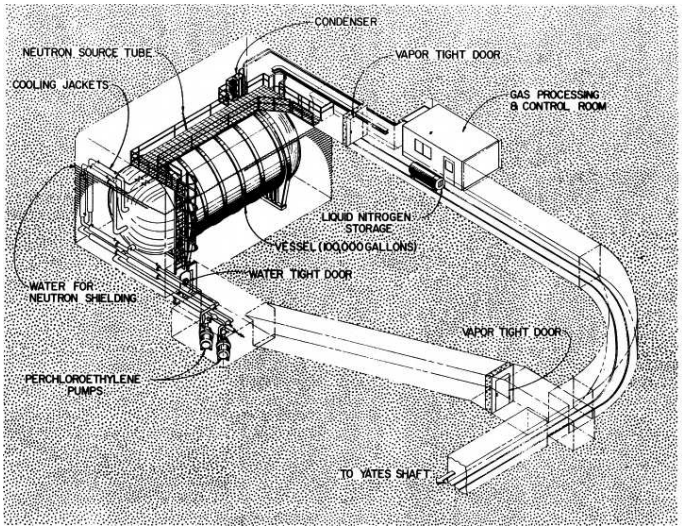

FIG. 2: The Chlorine detector in the Homestake mine.

The detector is sited underground to reduce ^{37}Ar production by cosmic rays. Detector and proportional counter materials were carefully selected to minimize contributions from background radioactivity. Background rates of ^{37}Ar from sources other than the Sun were restricted to about 0.02 atoms per day. Non-radioactive tracer isotopes ^{36}Ar and ^{38}Ar are injected during successive runs to determine the argon extraction efficiency and are measured by mass spectrometry. Pulse shape analysis is used on the pulses from the proportional counter to reduce counter backgrounds from other than ^{37}Ar decay.

The detector has been operated from 1968 until 2002 and the cumulative average of the data [1] is $2.56 \pm 0.16(stat) \pm 0.16(syst)$ SNU, where a Solar Neutrino Unit (SNU) is defined as one electron neutrino capture per 10^{+36} atoms of ^{37}Cl per second. This result is substantially smaller than the predictions of Standard Solar Models, for which the latest prediction [7] is $7.6^{+1.3}_{-1.1}$. The capture reaction on ^{37}Cl is calculated to be sensitive primarily to neutrinos from ^{8}B decay in the Sun, but there is substantial sensitivity to neutrinos from ^{7}Be as well. The expected contributions from the various SSM

calculated fluxes are shown in Table I .

2. Ga-Based Experiments: SAGE, GALLEX, GNO

The electron neutrino capture reaction on Ga (^{71}Ga(ν_e,e$^-$)^{71}Ge) has a threshold of 232 keV, well below the maximum energy of the neutrinos from the pp reaction in the Sun. Therefore detectors based on this medium have significant sensitivity to pp neutrinos as can be seen in Table I. Experiments with Ga as the detector material are being carried out in the Baksan laboratory in Russia (SAGE) [9] with about 60 tons of liquid Ga metal and in the Gran Sasso laboratory in Italy (GALLEX, GNO) [10] with 30.3 tons of Ga in a concentrated $GaCl_3$-HCl solution. The underground depths correspond to about 4700 meters of water equivalent for the SAGE experiment and 3300 meters for GALLEX and GNO.

The technique for detection of the neutrino reaction involves the observation of the radioactive decay of ^{71}Ge (half-life 11.4 days) by extraction and deposition into low-background proportional counters. For SAGE, the Ge is removed by extraction into an aqueous solution via an oxidation reaction, followed by concentration, conversion to $GeCl_4$ and synthesis to GeH_4 for use in the proportional counter. For GALLEX and GNO, volatile $^{71}GeCl_4$ is formed directly in the target solution, swept out by nitrogen gas, absorbed in water and then converted to GeH_4 before insertion into the proportional counter. The K and L electron capture decay of ^{71}Ge is observed through the energy deposition from the Auger electron and X-rays emitted in the decay. Detector materials are very carefully selected to minimize background counting in the proportional counter. Pulse shape discrimination is used to distinguish the highly-localized pulses from electron capture from the spatially-extended tracks from higher energy electrons associated with background processes.

Non-radioactive isotopes of Ge are inserted into the detector media and extracted along with the ^{71}Ge to monitor extraction efficiency. Analysis of the counting rates includes fitting a component with the characteristic half-life of ^{71}Ge as well as for background components including cosmogenically-produced ^{68}Ge (half-life 271 days) and other long-lived backgrounds. Special precautions are taken in each of the experiments to reduce contributions from ^{222}Rn (3.8 days) to a very small level. The experiments have used intense ^{51}Cr sources [11] to calibrate directly the sensitivity of the detector to neutrinos.

The counting rates from these two measurements to date [9, 10] are as follows: GALLEX + GNO: $70.8 \pm 4.5(statistical) \pm 3.8(systematic)$ SNU, SAGE: $70.9 + 5.3/-5.2(stat) + 3.7/-3.2(syst)$ SNU. These numbers are in excellent agreement and are much smaller than the predictions of the standard solar model (132 SNU) as shown in Table I.

D. Real-Time Solar Neutrino Detectors

1. Kamiokande and Super-Kamiokande

As described in Section 3, the Kamiokande detector, 1000 meters underground (2600 meters water equivalent) in the Kamioka mine in Japan, started operation in 1983 with the primary objective to study proton decay in a large light water volume. The detector had a fiducial volume of about 1 kton for the study of high energy events, including events produced by atmospheric neutrinos. After several years of operation, it was decided to add the additional capability of detecting solar neutrinos by improvements to the detector systems, particularly the electronics systems and the anti-counter system with full solid angle coverage. The detection reaction was elastic scattering of neutrinos from electrons, observed by the detection of Cherenkov light from the recoiling electron as discussed in Section 3. For the much lower energy solar neutrino measurements, the central region of light water (680 tons) was used and an energy threshold of about 7.0 MeV was achieved, limited primarily by gamma rays from residual radioactivity in the water, particularly ^{222}Rn. With this threshold, the solar neutrino sensitivity of the detector was almost exclusively for neutrinos from ^{8}B decay, with the neutrinos from the ^{3}Hep reaction expected to make a tiny contribution. A set of careful calibrations were carried out, including the use of radioactive sources of gamma rays.

The elastic scattering reaction has a strong directional dependence, peaked away from the direction of the incoming neutrino. A substantial excess of events from the Sun was observed, clearly distinguishable from background events and confirming the solar origin of the neutrinos. The flux of neutrinos from the ^{8}B decay was deduced [12] to be $2.8 \pm 0.19(stat) \pm 0.33(syst) \times 10^{+6}$ cm^{-2} s^{-1}, clearly less than the solar model prediction [7] of $5.05 \times 10^{+6}$ cm^{-2} s^{-1}. There was no evidence for variation in the flux as a function of time within the uncertainties.

The success of the Kamiokande detector prompted the construction of a much larger Super-Kamiokande detector nearby in the same mine as shown in Figure 3. After completion of the Kamiokande experiment, the detector was dismounted, the cavern enlarged and a new liquid scintillator experiment, KamLAND, with 1 kton target mass constructed. The objective of KamLAND is the detection of electron anti-neutrinos ($\bar{\nu}_e$) from distant nuclear power reactors to probe the solar large mixing angle parameter space. Data taking commenced in early 2002 and first results have been published [13].

A detailed description of the Super-Kamiokande detector is given in the section on atmospheric neutrinos below. For solar neutrino detection via the elastic scattering of neutrinos, the fiducial volume in the Super-Kamiokande detector is 22.5 kton. Considerable care was taken to reduce the radioactive backgrounds in the detector during construction. With this improved detector,

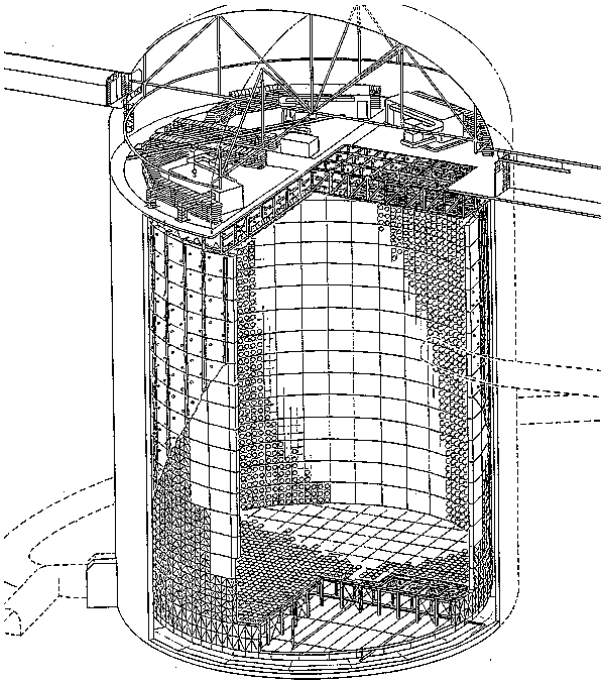

FIG. 3: The Super-Kamiokande detector.

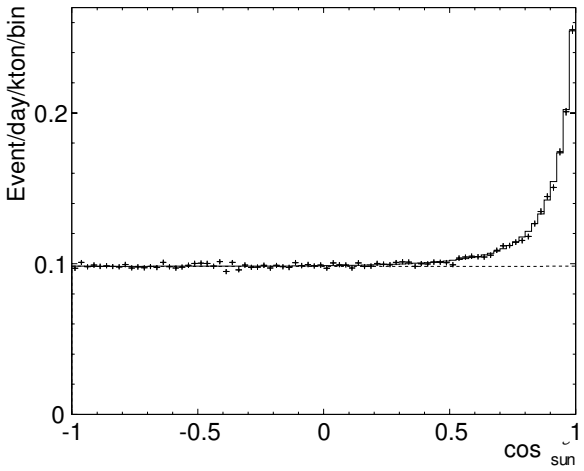

FIG. 4: Angular distribution of events from the Super-Kamiokande detector with respect to direction from the Sun.

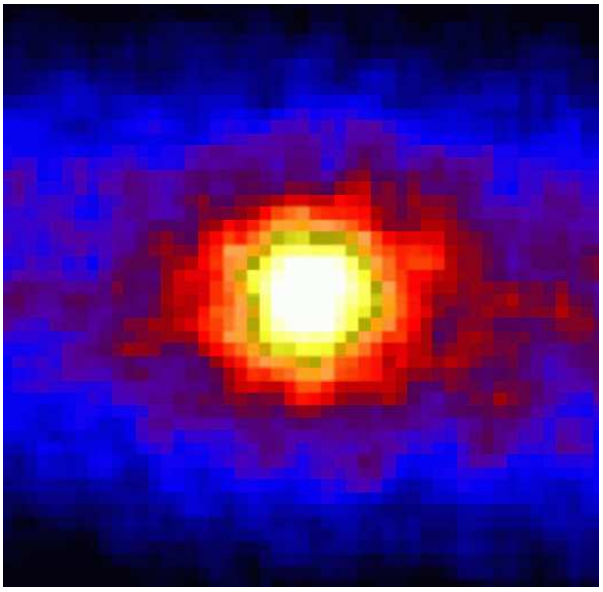

FIG. 5: Neutrino profile of the Sun obtained by the Super-Kamiokande detector. One pixel corresponds to one degree, which may be compared to the 1/2-degree apparent size of the sun. The distribution of colors is determined by the angle of neutrino-electron scattering.

the counting rate was increased substantially and additional improvements were made in calibration through the use of an electron linac. Figure 4 shows the data obtained for 1496 days of counting [6] versus the direction from the Sun for a threshold of about 5 MeV. The excess events from the Sun are clearly observable. Figure 5 shows a map of the Sun obtained with neutrinos detected by Super-Kamiokande.

The measured solar neutrino flux from ^{8}B decay is $2.35 \pm 0.02(stat) \pm 0.08(syst) \times 10^{+6}$ cm^{-2} s^{-1}, also significantly smaller than the solar model prediction. The neutrino energy spectrum is very similar to that expected from ^{8}B decay.

If there is a significant neutrino magnetic moment, this could couple with solar magnetic field distributions and produce different observed fluxes through flavor change as neutrinos pass through different solar regions at various times of year [14]. However, the neutrino flux as a function of time of year is observed to follow the variation expected for the Earth-Sun distance variation with no observable additional effects as shown in Figure 6. Studies over longer periods of time to seek correlations between the data and the sunspot numbers (indicative of magnetic fields in the outer regions of the Sun) also show no correlations [6].

Variation of the observed neutrino flux was also studied as a function of the zenith angle of events reaching the detector to search for effects of matter enhancement of flavor change while the neutrinos pass through the Earth. No clear effect was observed [6] as can be seen from the measurement of the fractional difference in the average rate in the day compared to the night: A $= -0.021 \pm 0.020(stat)^{+0.013}_{-0.012}(syst.)$.

To this point, the data from the radiochemical and the light water detectors all showed a significant reduction in the detected neutrino flux compared to the standard solar models. Many studies were made of solar models to seek changes that could produce neutrino fluxes similar to those observed. As no obvious changes could be found to explain the neutrino measurements there was a strong indication that neutrino oscillations could be occurring. However, since the different experiments were sensitive to different combinations of fluxes from the solar reactions, analyses in terms of neutrino oscillations depended on

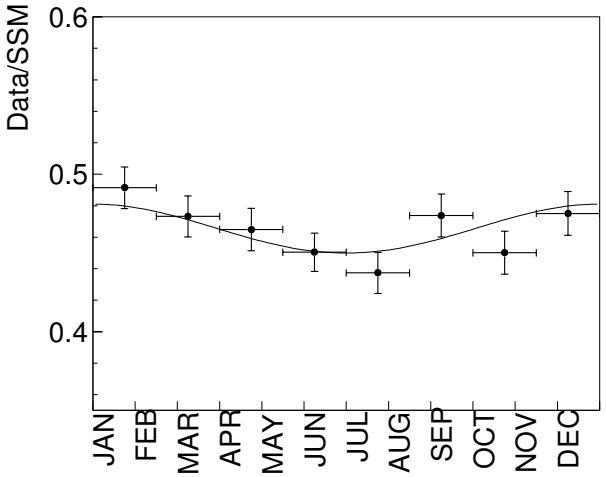

FIG. 6: Seasonal variation of the solar neutrino flux. The curve shows the expected seasonal variation of the flux introduced by the eccentricity of the Earth's orbit.

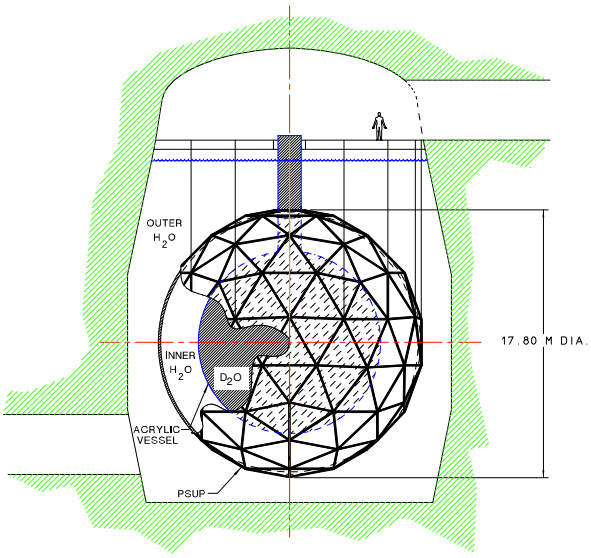

FIG. 7: Outline drawing of the SNO detector.

the correctness of solar models.

2. *Sudbury Neutrino Observatory*

The Sudbury Neutrino Observatory [15] is a real-time neutrino detector based on 1100 tons of heavy water sited 2000 meters underground (6200 meters water equivalent) near Sudbury, Ontario, Canada. Neutrinos are detected via the Cherenkov light produced by electrons moving faster than the speed of light in the central heavy water volume or in a surrounding volume of light water. As shown in Figure 7, the heavy water is contained in a 12 meter diameter transparent acrylic plastic vessel (AV) and the Cherenkov light is detected by 9456 20-cm photomultiplier tubes mounted on a 17.8 meter geodesic sphere (PSUP). The detector is contained within a polyurethane-lined cavity 22 meters in diameter by 34 meters high, filled with ultra-pure light water.

SNO measures the ^{8}B neutrinos from the Sun through the reactions:

$$\begin{aligned} \nu_e + d &\rightarrow p + p + e^- && \text{(Charged Current:CC)} \\ \nu_x + d &\rightarrow p + n + \nu_x && \text{(Neutral Current:NC)} \\ \nu_x + e^- &\rightarrow \nu_x + e^- && \text{(Elastic Scattering:ES)} \end{aligned}$$

The experimental objective is to use this combination of reactions to determine if electron neutrinos are changing their flavor, without reference to solar model calculations. The CC reaction is sensitive exclusively to electron neutrinos, while the NC reaction is sensitive to all neutrino flavors ($x = e, \mu, \tau$) above the energy threshold of 2.2 MeV. The ES reaction is sensitive to all flavors as well, but with reduced sensitivity to ν_μ and ν_τ. Comparison of the ^{8}B flux deduced from the CC reaction with the total flux of active neutrinos observed with the NC reaction (or the ES reaction with reduced sensitivity) can provide clear evidence of neutrino flavor transformation without reference to solar model calculations. If the neutrino flavor change process is occurring and can be fully understood, the original flux of electron neutrinos from the Sun can also be determined, providing an excellent test of solar model calculations.

The CC and ES reactions are observed through the Cherenkov light produced by the electrons. The electronic systems are designed to obtain a measure of the time of arrival and light intensity observed by each of the PMTs. The two dimensional projection of the Cherenkov cone on the array of PMTs and the arrival times provide a measure of the light intensity, origin and direction of the event. The NC reaction is observed through the detection of the neutron in the final state of the reaction. The SNO experimental plan involves three phases wherein different techniques are employed for the detection of neutrons from the NC reaction. During the first phase, with pure heavy water, neutrons are observed through the Cherenkov light produced when neutrons are captured on deuterium, producing 6.25 MeV gammas. For the second phase, about 2.7 tons of salt is added to the heavy water and neutron detection is enhanced through capture on Cl, with about 8.6 MeV gamma energy release and higher capture efficiency. In the third phase, the salt is removed and an array of ^{3}He-filled proportional counters is installed to provide neutron detection independent of the PMT array.

The SNO detector was constructed from carefully chosen, low-radioactivity materials. All workers took showers and used lint-free clothing to maintain Class 2000 air quality during construction. The water systems include processes for purifying the light and heavy water and measuring the residual radioactivity accurately. During operation, radioactivity levels were achieved that result in background events for the NC reaction that are less than 5% of the predicted rate from the Standard Solar

Model neutrino flux. The threshold for observation of the CC and ES reactions is 5 MeV in equivalent electron energy.

Results from the initial phase of the experiment with pure heavy water [5, 16, 17] show clear evidence for neutrino flavor change, without reference to solar model calculations. The data from this phase is shown in Figure 8, together with the best fit to the data of the NC (6.25 MeV gamma) shape, the CC and ES reactions assuming an undistorted shape for the ^{8}B neutrino spectrum and a small background component determined from independent measurements.

The fluxes inferred for this fit are:

$$\begin{aligned}
\phi_{\rm CC}^{\rm SNO} &= 1.76^{+0.06}_{-0.05}({\rm stat.})^{+0.09}_{-0.09}\ ({\rm syst.}) \\
\phi_{\rm ES}^{\rm SNO} &= 2.39^{+0.24}_{-0.23}({\rm stat.})^{+0.12}_{-0.12}\ ({\rm syst.}) \\
\phi_{\rm NC}^{\rm SNO} &= 5.09^{+0.44}_{-0.43}({\rm stat.})^{+0.46}_{-0.43}\ ({\rm syst.}).
\end{aligned}$$

where these fluxes and those following in this section are quoted in units of 10^6 cm^{-2} sec^{-1}. A simple change of variables resolves the data directly into electron (ϕ_e) and non-electron ($\phi_{\mu\tau}$) components. This change of variables allows a direct test of the null hypothesis of no flavor transformation ($\phi_{\mu\tau} = 0$) without requiring calculation of the CC, ES, and NC signal correlations.

$$\begin{aligned}
\phi_e &= 1.76^{+0.05}_{-0.05}({\rm stat.})^{+0.09}_{-0.09}\ ({\rm syst.}) \\
\phi_{\mu\tau} &= 3.41^{+0.45}_{-0.45}({\rm stat.})^{+0.48}_{-0.45}\ ({\rm syst.})
\end{aligned}$$

assuming the standard ^{8}B shape.

Combining the statistical and systematic uncertainties in quadrature, $\phi_{\mu\tau}$ is $3.41^{+0.66}_{-0.64}$, which is 5.3σ above zero, providing strong evidence for flavor transformation consistent with neutrino oscillations [3]. Adding the Super-Kamiokande ES measurement of the ^{8}B flux [6] $\phi_{\rm ES}^{\rm SK} = 2.32 \pm 0.03({\rm stat.})^{+0.08}_{-0.07}$ (syst.) as an additional constraint, we find $\phi_{\mu\tau} = 3.45^{+0.65}_{-0.62}$, which is 5.5σ above zero.

The total flux of ^{8}B neutrinos measured with the NC reaction is in very good agreement with the SSM prediction [7] of $5.05 \pm 1.0 \times 10^6$ cm^{-2} s^{-1}.

(Note added in proof: The SNO collaboration has recently reported [18] results from the second phase of the experiment where sodium chloride was added to the heavy water. The neutrons from the NC reaction capture on Cl and provide a more isotropic pattern at the PMT's for these events than for the CC events. This enables the fluxes from the CC and NC reactions to be determined independently with no constraint on the shape of the CC energy spectrum. The results are in good agreement with the previous constrained measurements and the total flux of ^{8}B neutrinos inferred from the NC reaction was determined to be 5.21 ± 0.27 (stat) ± 0.38 (syst) $\times 10^6$ cm^{-2} s^{-1}. This determination of the ^{8}B flux is independent of the presence of oscillations to active neutrino types and is in very good agreement with SSM predictions.)

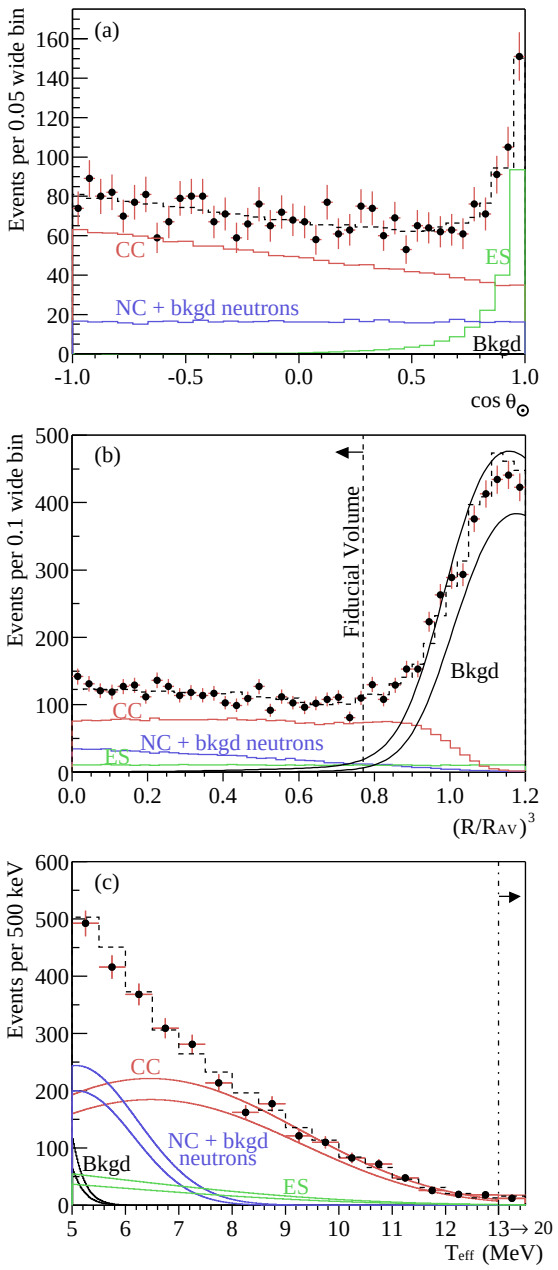

FIG. 8: (a) Distribution of $\cos\theta_\odot$ for $R \leq 550$ cm. (b) Distribution of the volume weighted radial variable $(R/R_{\rm AV})^3$. (c) Kinetic energy for $R \leq 550$ cm. Also shown are the Monte Carlo predictions for CC, ES and NC + bkgd neutron events scaled to the fit results, and the calculated spectrum of Cherenkov background (Bkgd) events. The dashed lines represent the summed components, and the bands show $\pm 1\sigma$ uncertainties.

E. Summary of Results from Solar neutrino telescopes to date

The measurements to date (see Table II) have provided convincing evidence for flavor change of neutrinos and matter enhancement of these effects in the Sun. If all

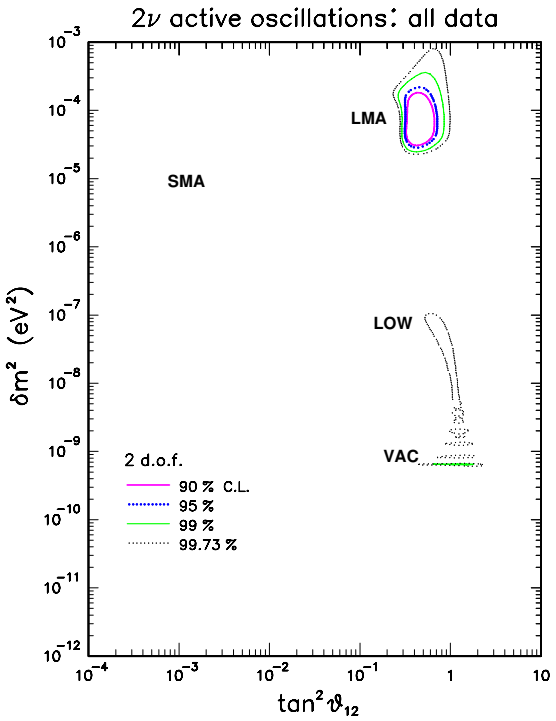

FIG. 9: Global fit to all the solar neutrino data in terms of a two-neutrino MSW oscillation scenario [19]

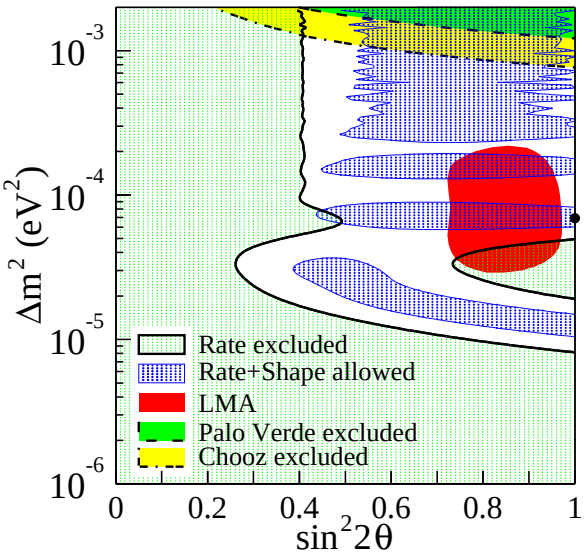

FIG. 10: Allowed regions of anti-neutrino oscillation parameters for the rate analysis and the combined rate and shape analysis from KamLAND at 95% confidence limit. Also shown are the LMA region allowed by solar neutrino measurements and excluded regions from CHOOZ and Palo Verde reactor neutrino experiments.

the measurements are combined in a global fit [19] to the neutrino oscillation process (assuming 2 neutrino oscillation), the remaining allowed regions are shown in Figure 9. These regions are labeled LMA, LOW and VAC, and the most favored among them is the LMA region. Recent measurements [13] reported by the KamLAND experiment using reactor anti-neutrinos provide substantial support for the LMA region as shown in Figure 10. Future solar neutrino measurements will seek to improve on the definition of these neutrino properties as well as studying further the spectrum of electron neutrinos from the Sun, as discussed in more detail in the following section.

III. FUTURE SOLAR NEUTRINO EXPERIMENTS

With the observation of flavor conversion by the combined analysis of SNO (CC) and Super-Kamiokande (ES), and by SNO(NC+CC) on its own, the scientific goals of upcoming experiments and future projects have shifted from discovery and identification of the solar neutrino flux deficit to a comprehensive study of the phenomena. The central challenge now is to measure, with high accuracy, neutrino oscillation parameters and to determine accurately the neutrino fluxes of the primary solar pp-, pep- and ^{7}Be branches. Beyond this clear cut goal, and despite the apparent consistency of observations with solar model predictions and oscillation scenarios, unexpected results might await and reveal further new physics.

Details of stellar evolution theory can be tested by comparing experimental neutrino fluxes with theoretical predictions [7, 8]. Most suited for such tests are the low energy pp-, pep- and ^{7}Be fluxes, since they are predicted with rather small theoretical uncertainties compared with the high energy ^{8}B: the pp- and pep-branch errors are estimated with 1% and 1.5% uncertainty, and the ^{7}Be line with 10% to be compared with 18% for the ^{8}B branch [20].

Oscillation solutions derived from solar neutrino data alone, allow two distinct parameter ranges, named LMA, LOW/VAC MSW-solutions and displayed in Figure 9. Including the recent results from the KamLAND experiment [13] into the global analysis [21] which reported evidence for the disappearance for $\bar{\nu}_e$ from nuclear reactors, and provided that CPT symmetry is not violated (ie. no difference in the disappearance probability $P(\bar{\nu}_e \rightarrow \bar{\nu}_x)$ and $P(\nu_e \rightarrow \nu_x)$, all but the LMA solution are excluded (cf. Figure 10). This solution makes distinct predictions for the electron neutrino survival probabilities of approximately 60 % for the pp-, pep- and ^{7}Be neutrino flux as diplayed in Figure 11. Details of the survival probabilities for pp-, pep-, ^{7}Be-, ^{8}B-, ^{13}N- and ^{15}O neutrinos as a function of energy are displayed in Figure 12 [22] for $\Delta m^2 = 7.1 \cdot 10^{-5} eV^2$ and $\sin^2 2\Theta = 0.41$. The relative shift of the survival probabilities for pp- and pep neutrinos with respect to eg. ^{7}Be is related to the different radial distribution of neutrino production inside of the

TABLE II: A summary of solar neutrino detectors referred to in section II, restricted to experiments that have published results.

Name	Dates	Location	Mass(Fid.)	Detector Details
Homestake [1]	1968 - 2001	Homestake mine, U.S.A.	0.7 kton	Perchlorethylene
SAGE [9]	1990 -	Baksan Laboratory, Russia	60 tons Ga	Gallium metal
GALLEX - GNO [10]	1990 -	Gran Sasso Laboratory, Italy	30 tons Ga	Gallium Chloride
Kamiokande III [12]	1983-1996	Kamioka mine, Japan	4.5(0.68) kt H_2O	1000 50-cm PMTs
Super-Kamiokande [6]	1996-	Kamioka mine, Japan	50(22.5) kt H_2O	11100 50-cm PMTs
SNO [15]	1998-	Creighton mine, Canada	1.1 (0.8) kt D_2O	9456 20-cm PMT's

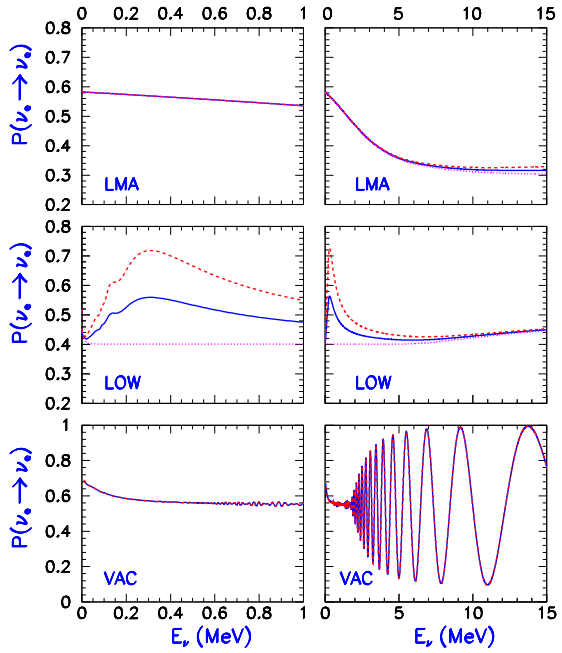

FIG. 11: Energy dependent survival probabilities for solar neutrinos for various oscillation scenarios. The distinct differences at energies below 1 MeV should be noted. The dashed, solid and dotted lines correspond to night, average and day spectra respectively [23]. Including the results from the KamLAND reactor neutrino experiment, all solutions but the LMA solution are excluded.

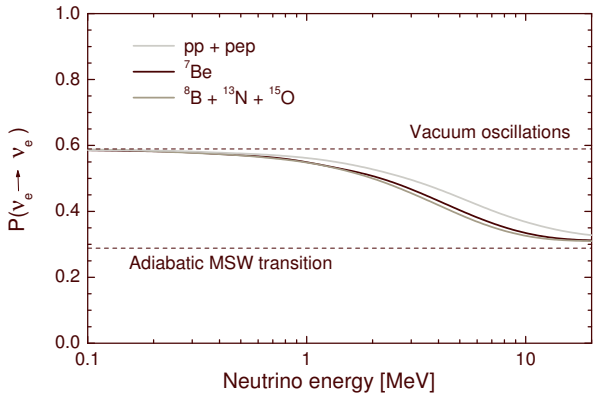

FIG. 12: Electron survival probabilities for pp-, pep-, ^{7}Be-, ^{8}B-, ^{13}N- and ^{15}O neutrinos for $\Delta m^2 = 7.1 \cdot 10^{-5}\text{eV}^2$ and $\sin^2 2\Theta = 0.41$.

sun, and thus to the difference in electron density during propagation of the neutrinos.

To address these fundamental issues of particle- and astrophysics, pp-, pep- and ^{7}Be neutrinos which are emitted in the predominant terminations of the solar fusion process, will be studied with new detectors that provide information about the energy and time of the neutrino interaction.

A. Real-time detection of low-energy solar neutrinos

Rigorous tests of particle properties, and simultaneously of solar model predictions, require measurements of the neutrino spectra for each flavour separately. The electron neutrino (ν_e) flux can be probed by the charged current inverse electron-capture reaction $\nu_e + (A, Z) \rightarrow e^- + (A, Z+1)^*$ (CC). Solar neutrinos, converted to muon (ν_μ) and tau (ν_τ) neutrinos can not produce their charged lepton partners, because their restmasses are large compared to the energy available. However, the $\nu_{\mu,\tau}$ flux component can be derived from the combined analysis of inverse electron-capture detection with elastic electron scattering $\nu_{e,\mu,\tau} + e^- \rightarrow \nu_{e,\mu,\tau}$ (ES), as shown by SNO and Super-Kamiokande. The ES detection involves both charged and neutral current interactions, albeit the contribution of the latter to the cross section is only about 1/6. Therefore, high precision measurements are needed, in particular if only a fraction of the flux is converted to $\nu_{\mu,\tau}$'s.

The total flux of all active flavors - the quantity to be compared with solar model predictions - can only be derived by a combined analysis of CC and ES experiments. An exclusive neutral current detection technique, as for the high energy ^{8}B flux, is not at hand to be realized experimentally.

The Cherenkov technique for measuring solar neutrinos has been successfully used for ^{8}B neutrinos. However, at energies at 1 MeV or below, the Cherenkov pho-

ton yield is insufficient to perform spectroscopic measurements. For this reason, scintillation techniques will be used for the upcoming low-energy neutrino experiments. A primary photon yield of up to 1×10^4/MeV can be achieved for organic liquid scintillators and up to 4×10^4/MeV in liquid noble gases. Ultra pure liquid scintillators will be used for ES detection, while metal loaded organic scintillators for CC detection. The use of a Time Projection Chamber (TPC) is under study as an alternative to scintillation detection for ES with the goal to reconstruct the full kinematics of the ES reaction.

Only a few promising candidate nuclei exist for CC real time detection. Either the transition must populate an isomeric excited state with a subsequent electromagnetic de-excitation, or the final state needs to be unstable in order to provide a coincidence tag to discriminate against background events such as ES signals and radioactive decays. Moreover, the energy threshold of the transition needs to be sufficiently low to have sensitivity to sub-MeV neutrinos. Only a few isotope meet these requirements of which ^{115}In, ^{100}Mo, ^{82}Se, ^{160}Gd, ^{176}Yb are under careful consideration.

The SSM interaction rates (without flavor conversion) for ES experiments amount to about 0.5/ton/day for ^{7}Be-ν's (860 keV branch), to 2/ton/day for pp-neutrinos and 0.04/ton/day for pep-neutrinos. Hence target masses of about 100 ton are required for ^{7}Be- and pep-measurements, while about 10 tons are sufficient for pp-neutrinos in order to acquire a rate of ten events per day.

The interaction rates for CC detection via inverse electron capture depend on the nuclear structure of the isotope under consideration and its relative abundance. For example, the interaction rate in indium (^{115}In, matrix element $B(GT)$=0.17, 95.7% natural abundance) is 0.07/ton/day for ^{7}Be-ν's and 0.3/ton/day for pp-ν's assuming SSM fluxes without oscillations.

B. Backgrounds to neutrino detection at low-energies

The main challenge of real time neutrino detection at low energies are backgrounds from radioactive decays. Primordial radioactive contaminants present in detector materials such as ^{40}K, ^{238}U, ^{232}Th and their progenies, as well as anthropogenic ^{85}Kr, cosmogenic ^{39}Ar, and radiogenic ^{14}C dominate the detector signal if not removed carefully.

Scintillation based ES experiments rely on the detection of a single recoil electron. Therefore, any radioactive decay with similar energy deposition can mimick a neutrino event. Concentration of radioactive elements need thus to be $< 1\mu$Bq/ton to allow a signal/background ratio > 1. This translates to contamination limits $\lesssim 10^{-16}$g U(Th)/g for ^{7}Be detection. CC experiments typically require less strigent limits since delayed coincidence tags suppress backgrounds.

Further backgrounds arise from cosmic ray muon induced radio isotopes. To minimize this interference, detectors are located deep underground. A rock overburden, for example, of 3400 mwe (meters of water equivalent), as encountered at the Gran Sasso underground laboratories, reduces the muon flux to 1.1 h^{-1} m^{-2}. Despite a reduction of a factor 10^6 with respect to the sea level flux, the in-situ production of radio-isotopes by spallation reactions is still of relevance. For example, backgrounds to pep-neutrino detection via ES at this depth is dominated by in-situ production of ^{11}C ($t_{1/2}$ = 20.4 min) by muons and their secondary particles. The ^{11}C production (and decay) rate amounts 0.15/ton/day to be compared to 0.04/ton/day pep-neutrino interactions [24]. Therefore, efficient spallation cuts, or alternatively, a deeper underground location are required to extract a pep-neutrino signal.

C. Upcoming experiments

The Borexino experiment is the pioneering project for real time solar neutrino spectroscopy at low energies [25]. The construction of the experimental installations is nearing completion in the underground laboratories at Gran Sasso, Italy (LNGS). Startup of the experiment is expected for 2004. The primary goal of Borexino is to measure the 0.86 MeV ^{7}Be-ν line via elastic neutrino–electron scattering (ES). Further physics goals include the detection of pep-neutrino, the low energy part of the ^{8}B spectrum, neutrinos from supernovae, as well as anti-neutrinos ($\bar{\nu}_e$) from distant nuclear reactors and from geophysical sources.

Fig. 13 displays schematically the Borexino detector. Neutrino detection occurs via ES in an ultra-pure liquid scintillator target confined in a transparent nylon vessel. The scintillator, with a mass of 300 tons (100 tons fiducial volume) is composed of pseudocumene (PC) and PPO at a concentration of 1.5 g/l. About 10^4 primary photons/MeV are emitted with a wavelength distribution peaked at 380 nm. Photon detection is realized with 2200 photomultipliers (8", 30% coverage) at single photoelectron threshold providing a yield of $\gtrsim$ 400 photoelectrons/MeV. An energy resolution of $\gtrsim$ 5% (1σ) at 1 MeV is therefore attainable. The location of the interaction within the detector is determined with an uncertainty of $\lesssim$ 10 cm (1σ) at 1 MeV using the time-of-flight method of the photons.

A trigger is generated by $\approx 15-20$ PMT hits occurring in a time window of 60 ns corresponding to a threshold of about 50 keV energy deposition. The analysis threshold for recoil electrons from ^{7}Be-ν ES will be at 250 keV, depending on the actual ^{14}C activity in the scintillator.

To achieve the ultra-low background rate within the fiducial inner volume, the detector has an onion-like structure with increasing radio purities from outside to inside. γ-rays coming from detector components outside the scintillation volume are attenuated by the buffer liq-

uid surrounding the active volume. The final reduction of external activity is achieved by the outer layer of the liquid scintillator ("self-shielding"), defining a fiducial mass of 100 tons.

The cumulative background rate internal to the liquid scintillator must be $\lesssim 1 \times 10^{-6}\,\mathrm{s}^{-1}\,\mathrm{m}^{-3}$ in the neutrino analysis window between 250 keV and 800 keV. This translates to limits $\lesssim 10^{-16}$g/g for uranium and thorium, and their progenies (assuming secular equilibrium), to $\lesssim 10^{-14}$g/g for potassium, to $\lesssim 10^{-10}$g /g for argon and to $\lesssim 4\times10^{-16}$g/g for krypton. Due to the high mobility of radioactive noble gases, in particular ^{222}Rn, ^{39}Ar, ^{85}Kr, ultra-high vacuum leak-tightness standards of the system is required and gases in contact with the liquid scintillator, such as nitrogen need to be purified. A further source of backgrounds comes from surface deposition of ^{222}Rn progenies on detector components which are subsequently in contact with the liquid scintillator. In particular the buildup of ^{210}Pb ($t_{1/2} = 22.3$ yr) must be controlled since it feeds the decays of ^{210}Bi ($t_{1/2} = 5$ d) and ^{210}Po ($t_{1/2} = 138$ d) which create signals in the neutrino energy window.

All materials have been screened with high-purity germanium spectroscopy, and selected for low radioactive trace contaminants [26]. Surfaces which are in contact with the liquid scintillator have been tested for radon emanation, and are specially treated to remove ^{210}Pb and ^{210}Po deposits.

The detector concept and in particular, the attainable radioactive trace contaminations have been studied in a pilot experiment, the Counting Test Facility at Gran Sasso (CTF) [27]. During construction and startup of Borexino, the CTF serves as a sensitive instrument to verify the performance of the ancillary plants, such as the liquid handling distribution, the various purification systems, as well as the purity levels of PC prior to filling the Borexino detector.

A similar detector, however larger in size, has been realized by the KamLAND collaboration in the Kamioka mine in Japan [28]. The main objective of this experiment is to probe the oscillation parameter space of the solar MSW large mixing solution with electron antineutrinos ($\bar{\nu}_e$) from distant nuclear reactors. Radio purity requirements for $\bar{\nu}_e$-detection are less stringent compared to solar neutrino detection via ES. Data taking with reactor neutrinos started early 2002 and first results have been published [13]. In a second phase, with an upgraded liquid handling and purification system, it is intended to measure solar ^{7}Be neutrinos, provided that trace contaminations are at levels as required for Borexino.

The active volume of the KamLAND detector consists of 1000 ton of liquid scintillator composed of PC, mineral oil (dodecane) and PPO (1.5 g/l). An energy resolution of $\sim 7\%$ (1σ) at 1 MeV has been reported and is expected to improve to $\sim 6\%$ in the final detector configuration. First results on ^{238}U, ^{232}Th were $(3.5 \pm 0.5) \times 10^{-18}$ g/g, $(5.2 \pm 0.8) \times 10^{-17}$ g/g, while impurities such as ^{85}Kr and ^{210}Pb still need to be reduced substantially to allow ^{7}Be-ν detection.

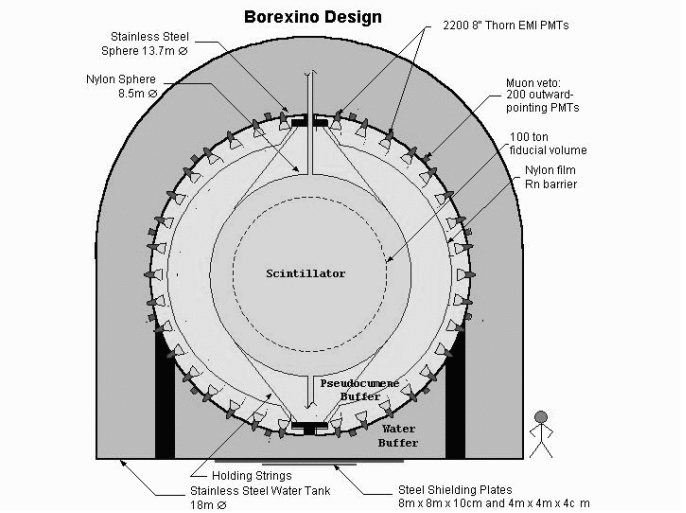

FIG. 13: Schematic view of the Borexino detector at Gran Sasso. A stainless steel sphere confines the inner detector (ID) containing about 300 ton liquid scintillator and 1 kton of transparent buffer liquid. Scintillation photons are detected by 2200 photomultiplier giving energy and location of the interaction. A fiducial central mass of 100 ton can be determined in the off-line analysis. The steel sphere is housed in a water tank equipped with 210 photomultiplier. The outer detector (OD) serves as a shield against ambient radiation as well as a muon track detector.

D. Next generation experiments

^{14}C/^{12}C ratios at 10^{-18} in organic scintillators, as determined with the CTF [30], prohibit the measurement of pp-neutrinos in ES experiments since the 156 keV β-decay endpoint significantly obscures the pp-neutrino energy range. A promising approach to overcome this background is to avoid organic liquids and instead, to use liquefied noble gas as a scintillator. Projects with helium, neon and xenon are under investigation and are listed in Table III. Recent development for pp- and ^{7}Be CC detection focuses on the isotopes ^{115}In (LENS) and on ^{100}Mo (MOON). Most advanced amongst the various R&D projects, listed in Table III, are XMASS for ES- and LENS for CC detection. In the following, experimental and conceptional details will be outlined for these two projects, exemplary for the next generation of experiments. Further details of recent progress of the various projects can be found at [31, 32].

The XMASS [35] collaboration pursues the concept of pp- and^{7}Be-ν detection via ES in a liquid xenon scintillation detector. High density liquid xenon (3.06 g/cm^3) provides efficient self shielding and a compact detector design. A geometry similar to that of Borexino, but smaller in size, could thus be realized. The scintilla-

TABLE III: R&D projects for sub-MeV solar neutrino detection. ES: Elastic scattering of neutrinos off electrons (CC+NC), CC: neutrino capture (charged current; CC); LS: liquid scintillator; CH: hydro-carbon

Project	Method	Technique (Target)
LENS [33]	CC: ^{115}In,^{176}Lu	LS (CH+metal)
MOON [34]	CC: ^{100}Mo	hybrid or LS (CH+metal)
XMASS [35]	ES	LS (Xe)
HERON [36]	ES	LS (He)
CLEAN [37]	ES	LS (He,Ne)
TPC [38]	ES	TPC(He,CH)

tion photons (175 nm) will be detected with newly developed low-background photomultiplier tubes (Hamamatsu) consisting of a steel housing and a quartz window at liquid xenon temperatures ($\lesssim$ 165 K). Main sources of backgrounds arise from ^{85}Kr β-decay and from $2\nu-\beta\beta$ decay of ^{136}Xe. The first isotope must be less than 4×10^{-15}gKr/g. If the $\tau_{1/2}$ of ^{136}Xe is $\lesssim 8\times10^{23}$ years, as theoretically expected, then isotope separation is needed. A prototype detector containing 100 kg of liquid Xe is under construction. Milestones during this R&D phase will include the determination of the $2\nu-\beta\beta$ half-life and the optical properties of liquid xenon, such as the scattering length of scintillation light.

Various candidate nuclei are being investigated by the LENS [33] collaboration. The ongoing research focuses now on ^{115}In loaded into an organic liquid scintillator with 5-10% in weight. Complexing ligands under study include carboxylic acids, phosphor organic compounds as well as chelating agents. A detector containing about 10 tons of indium is under consideration. In order to discriminate against backgrounds, dominated by the β-decay of ^{115}In (Q_β = 496 keV, 0.26 Bq/g of In) and the accompanying Bremsstrahlung, a detector with high spatial granularity is required. This will be realized by a modular design. A basic module has a parallelopiped shape with a length of 2-3 m, determined by the absorption length of the liquid scintillator. The cross section of the module varies from 5×5 cm^2 to 10×10 cm^2 depending on metal loading, scintillator performance and further optimization criteria under study.

The nuclear matrix element $B(GT) = 0.17$, relevant for ν_e interaction, has been determined via the (p,n) reaction. This value is sufficiently accurate to evaluate the target mass necessary for the LENS detector. However, to derive the neutrino fluxes with accuracy $\sim 5\%$, it is planned to use an artificial ^{51}Cr neutrino source of several MCi strength to determine the neutrino capture cross section.

In order to study the detector performance as close as possible to the final detector geometry, the LENS Low-Background-Facility (LLBF) has been newly installed underground at the Gran Sasso Laboratories (LNGS). A low-background passive shielding system with 80 tons of mass, located in a clean room, can house detector modules with dimensions up to 70 cm $\times$ 70 cm $\times$ 400 cm. All shielding materials have been selected in order to minimize the intrinsic radioactive contamination. First results from the prototype phase are expected end of 2003.

E. Outlook

In near future, the detection of ^{7}Be and, conceivably pep-neutrinos via ES will be addressed by Borexino and by KamLAND. The next generation projects still have to pass the threshold from promising ideas to feasible experiments. Results from the ongoing prototype activities will show within the very near future which of the projects have the potential to be realized. On the long term, complementary measurements via ES- and CC detection are desirable for all neutrino branches in order to scrutinize solar models as well as neutrino properties.

IV. SUPERNOVA NEUTRINOS

Up to 99 % of the roughly 10^{53} ergs of energy released in type II and type Ib supernova is carried away by neutrinos. Many of the currently operating neutrino telescopes are capable of detecting these neutrinos and providing detailed information on such supernovae. The standard model for a type II supernova is a massive star that has reached a point in its evolution when the pressure from fusion reactions can not support the gravitational pressure of the outer regions. An inward collapse is initiated and proceeds until the central density reaches nuclear density at which time a bounce occurs and an outward shock wave is created. The interaction of this outward moving shock wave with the outer material contributes to an explosion, aided by energy deposited behind the shock wave from neutrinos created in the collapsing core.

Although there are many detailed models of supernova dynamics, the models share a number of generic features. These are illustrated in Figure 14 from an article by Burrows et al [39] that explores the potential for supernova neutrino detection by a number of different detectors. Neutrinos and anti-neutrinos of all active types are produced during a period lasting up to about 10 seconds. The average neutrino energies are typically 12 MeV for electron neutrinos, 15 MeV for electron anti-neutrinos and 18 MeV for the muon and tau neutrinos

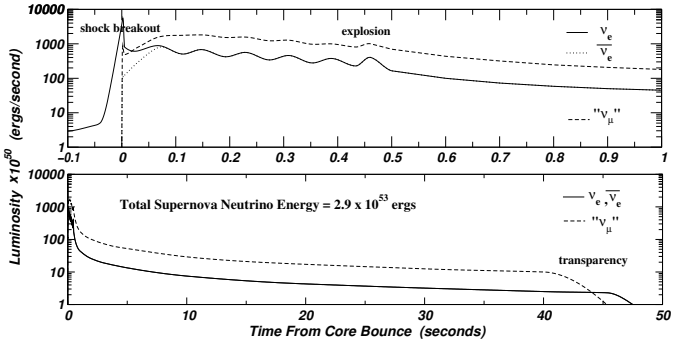

FIG. 14: (a) The luminosity (in ergs per s) vs time (in ms) for the ν_e, $\bar{\nu}_e$ and collectively, the $\nu_\mu(\bar{\nu}_\mu)$ and $\nu_\tau(\bar{\nu}_\tau)$ during the first second of the neutrino burst in the generic model employed by Burrows et al [39]. (b) Same as (a) but for the first 50 s.

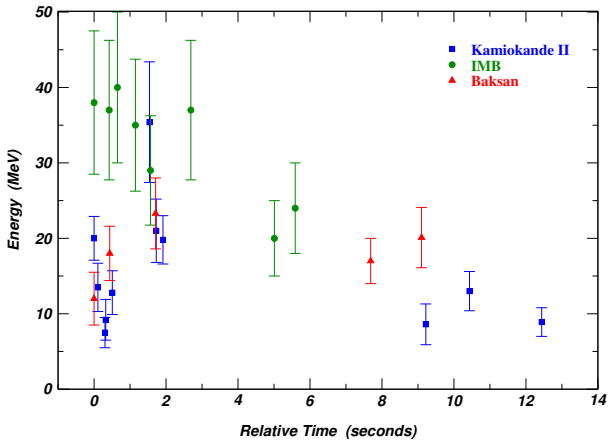

FIG. 15: Electron/positron energies and relative times for the events identified by the Kamiokande II, IMB, and Baksan detectors during SN1987a. The time of events recorded by each detector is relative to the first event in that detector [45].

and anti-neutrinos (labelled as mu neutrinos in the figure). The time period for neutrino generation can be divided into three principal regions, a collapse phase, an accretion phase and a cooling phase following an explosion. In the collapse phase electron capture on protons produces a sharp burst of electron neutrinos. When the core bounce occurs, neutrinos and antineutrinos are produced in the high temperature wake of the launched shock wave. Throughout the accretion phase, there is gradual spectral hardening of all the neutrino species that is increased sharply as an explosion occurs, reversing the flow of infalling matter and beginning the cooling phase during which the spectra soften again.

There are many detectors that have the capability to observe neutrinos from a Supernova in our galaxy or the Large Magellenic Cloud (LMC). This was demonstrated very dramatically when supernova 1987a was observed in three underground detectors. The Kamiokande, IMB and Baksan detectors observed neutrinos from this event that occurred in the LMC, about 51 megaparsecs from Earth [40, 41, 42, 43, 44]. Figure 15 shows the numbers, energies and arrival times of these neutrino events [45].

The detection process for these detectors is dominated by anti-electron neutrinos interacting with protons in water (2350 tons fiducial volume in Kamiokande, 5500 tons in IMB) or liquid scintillator (200 tons in Baksan). (A further 5 events were observed by the LSD detector but they occurred about 5 hours out of time with the other detectors.) The interactions on protons in these detectors has about ten times higher probability than elastic scattering from electrons, leading to the assignment of these events to this process with the highest probability. The events have been carefully analyzed and compared with models for supernova neutrino emission, with good agreement in general [44].

Experiments presently in operation or planned for the future have a broader capability for the detection of the next nearby supernova. The Super-Kamiokande detector has a fiducial volume of 32 ktons of light water and would provide significant signals for anti-electron neutrinos interactions with protons and all neutrino flavors interacting by elastic scattering on electrons. The SNO detector has a fiducial volume of 1.1 kton of heavy water and 1.5 kton of light water and can detect all neutrino types via several reactions. The LVD detector is a liquid scintilator detector with 1 kton fiducial mass. Supernova neutrinos are detected mainly through inverse beta decay: $\overline{\nu}_e p \rightarrow e^+ n$. In addition, neutrinos of all flavor can be detected by neutral current interactions off carbon, which produce mono-energetic 15.11 MeV gamma rays. Several other scintillator based detectors are in operation that are sensitive to inverse beta decay, including miniBooNE [46] and KamLAND.

The combination of detectors listed in Table IV from Burrows et al. [39] can provide a detailed measure of the flavor composition of the neutrino flux as a function of time, and energy to test models of supernovae. Neutrino flavor change processes can also occur during supernova and can be studied with the array of detectors now in operation. Because neutrinos can precede light emission from supernovae by as much as a few hours, it can be valuable to provide an advance signal from neutrino telescopes to other astronomical telescopes. Several of the existing experiments have formed a coordination group [47] known as the SuperNova Early Warning System (SNEWS) to look for coincident bursts of events among several of the experiments and provide as rapid a warning to other telescopes as possible. Whereas the timing of the leading edge of the neutrino burst provides only modest localization through triangulation [48], several of the experiments (SuperKamiokande and SNO) could provide localization to within a few degrees for a supernova near the galactic centre via the highly directional neutrino-electron elastic scattering reaction.

Few supernovae have been observed visually in our Galaxy in the past- about 6 in the past 1000 years. This

TABLE IV: Signal totals for various processes in representative supernova detectors at 10 Kpc [39]. ν_μ represents ν_μ, ν_τ, $\bar{\nu}_\mu$, $\bar{\nu}_\tau$.

Reaction	SNO	Superkamiokande	LVD
$\bar{\nu}_e$ p	331	5310	342
$\nu_e e^-$	12	77.6	8.04
$\bar{\nu}_e e^-$	6	16.9	1.49
$\nu_\mu e^-$	7	49.9	3.28
ν_eO (CC)	3	36.0	-
$\bar{\nu}_e$O (CC)	3	45.5	-
ν_xC	-	-	22
ν_ed (CC)	81.9	-	
$\bar{\nu}_e$d (CC)	66.7	-	
ν_ed (NC)	35.2	-	
$\bar{\nu}_e$d (NC)	37.2	-	
ν_μd (NC)	200	-	

is thought to be because most of them are obscured by intergalactic dust. Predictions of supernovae rates in our Galaxy range from one per 10 years to one per 100 years. The techniques used to make these estimates include estimates of stellar evolution rates, estimates based on iron abundances produced in supernovae, studies of supernovae rates in other galaxies and studies of supernova remnants. Detectors currently in operation have volumes providing sensitivity only out to the LMC region. A widely accepted range for the occurence rate is about one per 30 to 50 years in our galaxy and the LMC combined [49, 50]. Detectors capable of reaching far enough to obtain a rate of about one supernova per year have been discussed, but a volume more than 100 times the present detectors would have to be instrumented with a detection threshold on the order of about 10 MeV. Arrays of neutron detectors have also been considered but the total volume is a daunting task.

Large neutrino detectors may also be sensitive to so-called relic supernova neutrinos. These originate from sum of all distant supernovae, and appear as a relatively low background of interactions rather than as the brief burst of events characteristic of a nearby core collapse. Detailed predictions depend on the cosmological model that determines the average redshift and epoch of maximum supernova rate [51], and include the effects of neutrino oscillation. As with nearby supernovae, the most promising reaction is through the inverse beta decay reaction of $\bar{\nu}_e$. The flux of $\bar{\nu}_e$ is predicted to be rather small: less than 50 $\mathrm{cm}^{-2}\mathrm{s}^{-1}$ over the entire spectrum. This is 10^5 times smaller than the ^{8}B solar neutrino flux, which therefore offers a sizeable background.

In searches performed so far, the signal is sought in an energy window above the ^{8}B endpoint of 18 MeV and below the onset of numerous atmospheric neutrino interactions around 50 MeV. In this window there are still challenging backgrounds due to Michel electrons from untagged muon decays (such as from ν_μ interactions with the muon below a Cherenkov detection threshold), and low energy atmospheric ν_e interactions. The most recent studies are from Super-Kamiokande [52], which performed a combined signal and background fit to the energy spectrum in this region. No appreciable signal was detected in 92 kton-years and they limit the flux of relic supernova $\bar{\nu}_e$ to be less than 1.2 $\mathrm{cm}^{-2}\mathrm{s}^{-1}$ above $E_\nu > 19.3$ MeV.

V. ATMOSPHERIC NEUTRINO DETECTORS

In the early 1980's, the first massive (of order 1 kton) underground detectors were constructed, primarily to detect proton decay with a lifetime of less than 10^{32} years, as predicted by early Grand Unified Theories [53, 54]. The most serious background for proton decay searches is from atmospheric neutrinos, at a rate of approximately 100 events/yr/kt. Atmospheric neutrinos are produced as decay products in hadronic showers resulting from the collision of cosmic rays with nuclei in the upper atmosphere. The study of atmospheric neutrinos is interesting apart from background studies, as they provide a sample of muon and electron neutrinos that travel distances ranging from 10 km to 13000 km, thereby providing for the study of neutrino oscillation. Table V summarizes some of the experiments to date that have studied atmospheric neutrinos.

Atmospheric neutrinos interact with the nucleus, at a typical energy of 1 GeV, although the detectable spectrum extends beyond 1 TeV. In order to reject background from cosmic ray muons, as well as to reconstruct the details of the event cleanly, the vertex position of the neutrino interaction is typically required to be within some fiducial volume. There are several standard categories of events determined by the extent of the final state particles. Low energy events, around 1 GeV have all of the final state particles "fully contained" in the detector. Electromagnetic showers, even at energies of 10-100 GeV, are also usually fully contained. By placing energy or momentum cuts on the events, one may statistically define sub-samples of lower or higher average neutrino energy. A cut around 1 GeV (suitable for identifying proton decay), has traditionally demarked "sub-GeV" and "multi-

TABLE V: A summary of atmospheric neutrino detectors, restricted to experiments that have published results on a sample of at least 100 atmospheric neutrinos. If a detector was upgraded, the final name and configuration is listed; however the earliest start date for any version of the experiment is provided. The first section lists fine grained tracking detectors and the second section lists water Cherenkov detectors.

Name	Dates	Location	Mass(Fid.)	Detector Details
Baksan [56]	1978-	Baksan Laboratory, Russia	0.33(-) kt	Liq. scintillator tanks
Frejus [55]	1984-1988	Frejus tunnel, France/Italy	0.9(0.7) kt	Flash/geiger + iron planes
Soudan 2 [62]	1989-2001	Soudan iron mine, U.S.A.	0.96(0.77) kt	Drift tubes + corrugated steel
MACRO [63]	1988-2001	Gran Sasso Laboratory, Italy	4.7(-) kt	Streamer tube + liq. scint.
Kamiokande III [57]	1983-1996	Kamioka mine, Japan	4.5(1.0) kt	1000 50-cm PMTs
IMB 3 [58]	1982-1991	Morton Salt mine, U.S.A.	8.0(3.3) kt	2048 20-cm PMTs
Super-Kamiokande [64]	1996-	Kamioka mine, Japan	50(22.5) kt	11100 50-cm PMTs

GeV" data samples. Higher energy charged current ν_μ interactions may result in the muon exiting the detector; these are referred to as "partially contained". Some of the experiments are equipped with outer detectors (also referred to as veto- or anti-detectors) to easily identify exiting particles, as well as to reject cosmic ray background.

The other possible background source for contained events are high energy neutrons from muon interactions nearby the detector; this is a potentially more serious background, because neutrons enter a detector without any visible tracks. It has been reported that such neutron backgrounds may be controlled by a sufficiently thick active shield; one may then veto nearby cosmic ray muons that produce neutrons [65, 66].

There is a third category of charged current ν_μ events, where the interaction occurs outside the detector, and the muon enters and either passes through the detector or stops in the detector. These are referred to as "upward-going muons" because one generally requires they originate from below the horizon to ensure that a sufficient amount of rock absorbs ordinary cosmic ray muons (at very deep locations, especially with a flat overburden, the zenith angle requirement can be somewhat above the horizon [67]). Upward-going muons represent the highest energy neutrinos ($\sim$ 1 TeV) detected by atmospheric neutrino experiments, and have good pointing resolution ($\sim$ few degrees) with respect to the original neutrino direction. Therefore this sample is used for traditional neutrino telescope studies such as the search for astrophysical point sources [59] of high energy neutrinos including short duration sources such as gamma ray bursts [60]. In addition, dark matter annihilation in the sun, earth, and galactic center may produce neutrinos and the signal has been sought using upward-going muons [61]. All results to date have been negative, i.e. statistically consistent with only the expected background from atmospheric neutrinos (see also Section VI).

Figure 16 shows the distribution of parent neutrino energies for fully contained, partially contained, and upward-going muon event samples, specifically for the Super-Kamiokande analysis.

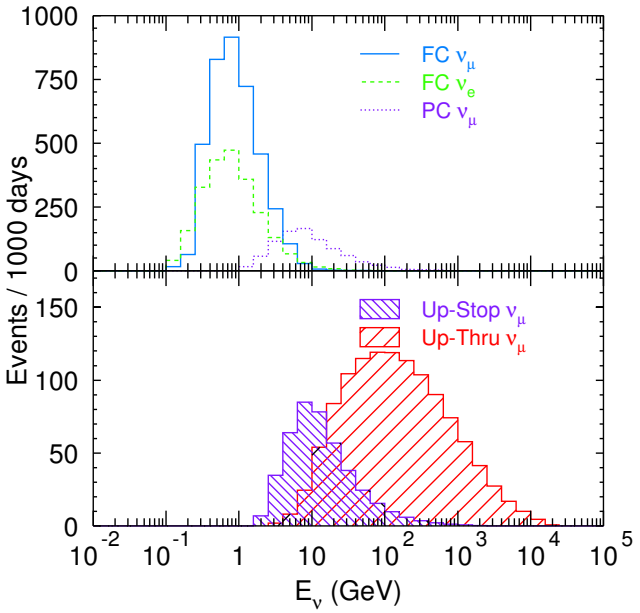

FIG. 16: The parent neutrino energy for several different classifications of atmospheric events. These distributions are for the Super-Kamiokande analysis; for other detectors they will be different depending on detector size, which controls the maximum energy of a fully-contained event and the minimum energy of a through-going muon.

A. Water Cherenkov Detectors

Atmospheric neutrino events are detected in water Cherenkov detectors by observing Cherenkov radiation from relativistic charged particles in the final state of the neutrino interaction. A two dimensional array of photomultiplier tubes on the inside surface of the detector detects the photons. The hit time and the pulse height from each PMT are recorded. The hit time, with a typical resolution of a few ns for a single photo-electron pulse, is used to reconstruct the vertex position. The total number of photo-electrons gives information on the energy of the particles above Cherenkov threshold. It is conventional to refer to "visible energy", which is defined as the equivalent energy assuming all of the Cherenkov

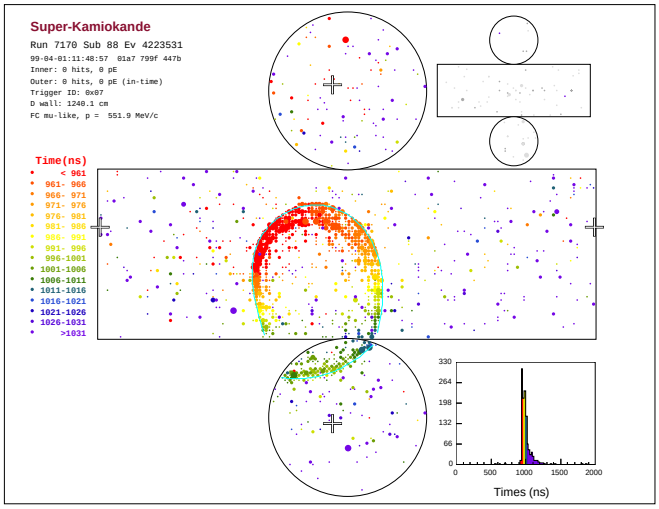

FIG. 17: An example event display from the Super-Kamiokande detector, showing the sharp-edged Cherenkov ring from a 0.6 GeV muon. Each small circle represents one PMT over threshold, with the size of the circle correlated with the number of photoelectrons, and the color of the circle related to the arrival time of the Cherenkov light.

light arises from electromagnetic showers. Thus, a muon of 1 GeV would produce about 0.9 GeV of visible energy, but an electron of 1 GeV would produce 1 GeV of visible energy. Figure 17 shows a fully-contained atmospheric neutrino event observed in the Super-Kamiokande detector.

It is possible to use the pattern of Cherenkov light to identify separately the electrons and muons produced by charged current ν_e and ν_μ interactions respectively. An electron produces an electromagnetic shower while propagating in a medium, and the low-energy electrons and positrons undergo multiple scattering while producing Cherenkov light. On the other hand, a muon propagates in a nearly straight line, losing energy by the ionization. In addition, the opening angle of the Cherenkov radiation is smaller for a low energy muon. These differences are used to form a likelihood for the Cherenkov pattern for electrons and muons. The nomenclature used is either e-like and μ-like or showering and non-showering.

The first generation water Cherenkov detectors were IMB and Kamiokande. IMB (originally named for Irvine-Michigan-Brookhaven) started taking data in 1982 and ended in 1991 after two major upgrades. The first phase of the detector (IMB 1) was equipped with 2048 12.5-cm diameter PMTs. The light collection was improved by the addition of 60 cm × 60 cm × 1.3 cm waveshifting plates [68], for a brief running period (IMB 2). Finally, the detector was equipped with 2048 20-cm PMTs, again with a wave length shifter plate (IMB 3). The Kamiokande detector (the name is based on Kamioka Nucleon Decay Experiment) used 1000 PMTs with 50-cm diameter, a photocathode coverage of 20%. For the second phase, Kamiokande had an outer detector with thickness of the water between 0.5 and 1.5 m. The outer detector made it possible to identify partially contained events. These experiments showed that the observed fraction of muons relative to electrons was much smaller than the Monte Carlo prediction [69, 70]. The Kamiokande result for multi-GeV and partially contained events suggested a zenith angle dependence indicative of neutrino oscillation [71].

The current generation water Cherenkov detector is Super-Kamiokande (see Fig. 3), whose results dominate our understanding of atmospheric neutrinos. It began taking data in 1996. Super-Kamiokande has a total mass of 50 ktons, with an inner detector 36 m in height and 34 m in diameter. It uses 11146 50-cm diameter PMTs, with photocathode coverage of 40% of the inner detector surface, a factor two higher than that of Kamiokande. An outer detector surrounds the inner detector with 2 m thickness of water, equipped with 1885 20-cm diameter PMTs with wavelength shifting plates (these were recovered from the IMB experiment). To limit the scattering of the Cherenkov photons, Super-Kamiokande has an extensive water purification system. As a result, the attenuation length of the water is longer than 100 m for 400 nm wavelength light. The fiducial volume for neutrino vertices is 2 m from the plane of photomultiplier tubes, resulting in a 22.5 ktons mass. The large mass and photocathode coverage allows for high statistics and detailed studies of atmospheric neutrinos. The misidentification probability of electrons and muons is about 1%. This high efficiency makes it possible to study details of CC ν_e and ν_μ events. Figure 18 shows the zenith angle distributions for contained atmospheric neutrino events. An energy and zenith angle dependent deficit of μ-like events is clearly visible. From these distributions, it was concluded that the observed data show a compelling evidence for neutrino oscillations [72].

Since the zenith angle distributions for e-like events show no evidence for inconsistency between data and non-oscillated Monte Carlo, it can be concluded that the oscillation could be between ν_μ and ν_τ. Indeed, detailed oscillation analyses of the Super-Kamiokande data [72, 73] have concluded that the data are completely consistent with two-flavor $\nu_\mu \rightarrow \nu_\tau$ oscillations. The present understanding of the oscillation parameters $(sin^2 2\theta,\ \Delta m^2)$ for $\nu_\mu \rightarrow \nu_\tau$ two flavor oscillation is shown in Figure 19. Results from 4 experiments are shown, and all the results are essentially consistent. The most accurate result from Super-Kamiokande gives oscillation parameters of: $\sin^2 2\theta > 0.92$ and $1.6 \times 10^{-3} < \Delta m^2 < 3.9 \times 10^{-3}\text{eV}^2$ at 90% C.L.

In addition, it is possible for water Cherenkov detectors to study more complicated events. An example of such events are those containing a single π^0. These events are characteristic of neutral current neutrino interactions, and are therefore useful in the study of neutrino oscillations to sterile neutrinos. Since the π^0 decays to two gamma rays, these events are comprised of two e-like ring events. Figure 20 shows the invariant mass distribution for two electron-like events. A clear peak is seen at the

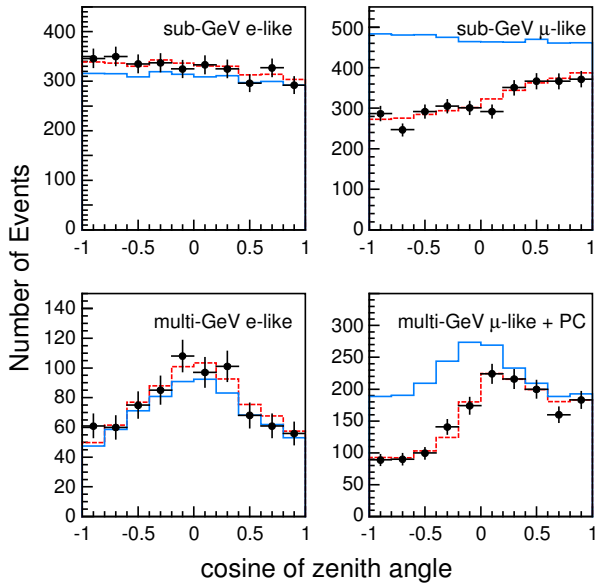

FIG. 18: Zenith angle distributions observed in Super-Kamiokande for sub-GeV e-like events(top-left), for multi-GeV e-like events(bottom-left), for sub-GeV μ-like events(top-right), and for multi-GeV μ-like plus partially-contained events(bottom-right). The solid lines show simulations for no neutrino oscillations, the dashed lines show the best fit assuming oscillations.

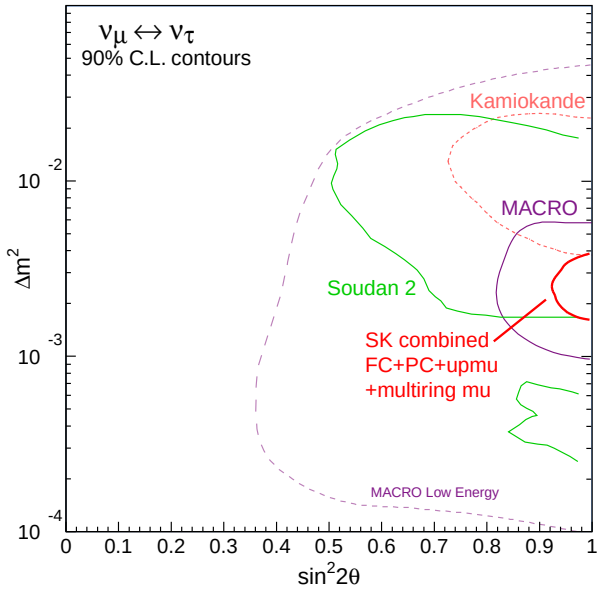

FIG. 19: 90% C.L. allowed parameter regions of oscillation parameters from Super-Kamiokande(thick line), Kamiokande(thick broken line), Soudan-2(thin line) and MACRO(thin broken line). Two flavor $\nu_\mu \rightarrow \nu_\tau$ oscillations are assumed.

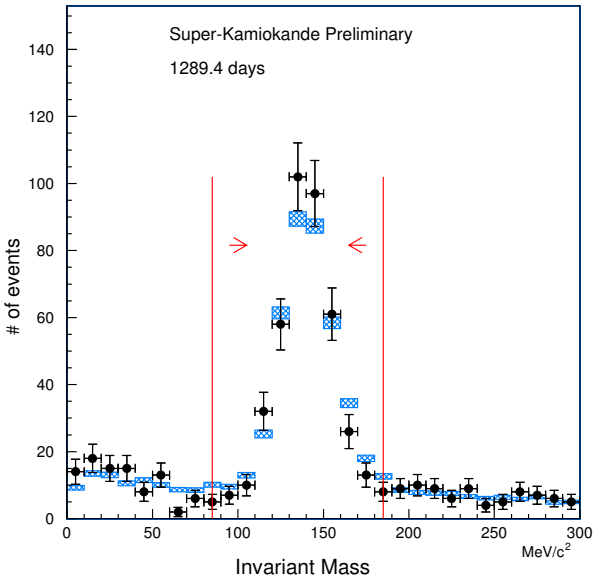

FIG. 20: Invariant mass distribution for two electron-like ring events observed in Super-Kamiokande based on 79 ktonyr data. Data are shown as filled circles, simulation as hatched rectangles.

π^0 mass.

It is possible to construct a water Cherenkov detector larger than Super-Kamiokande. It is widely thought that the next generation water Cherenkov detectors should have the mass of about 1 Mton, in order to carry out large statistics neutrino oscillation studies with neutrino beams, and in order to probe proton decay lifetimes approaching 10^{35} years, as predicted by modern Grand Unified Theories. These detectors would also observe significantly larger number of atmospheric neutrino events. By exploiting the high statistics and the up-down symmetry of the neutrino flux, it should be possible to determine $\sin^2 2\theta$ to an accuracy of about 1%. This is possible, because $N_{up}/N_{down} = 1 - \sin^2 2\theta/2$ to first approximation, where N_{up} and N_{down} show the number of upward going and downward going events. Since the dimension of the detector is larger, muons with energy higher than 10 GeV will be contained in the detector. It could then be possible to observe the "oscillation" nature of the ν_μ disappearance that has not been observed by any oscillation experiment. In addition, a larger detector with good ν_e reconstruction could observe the yet-unobserved mixing angle (θ_{13}) through the Earth-matter effect, if the mixing angle is near the present limit [75].

One of the technical requirements for such ultra-large water Cherenkov detectors was exposed in 2001 by the accidental loss of photomultiplier tubes by a chain reaction caused by a single imploding tube in the Super-Kamiokande detector. Detailed studies were subsequently performed, both with hydrodynamic computer simulations and in-situ tests under 4.5 atmospheres of water pressure. Based on these studies, a two-piece protective shell was designed, consisting of $\sim$ 8 mm fibre reinforced plastic and 13 mm clear acrylic. The shell is not intended to withstand static pressure, but has several small holes which allow water to form a layer between the PMT and the shell. If the PMT breaks, water rushes in

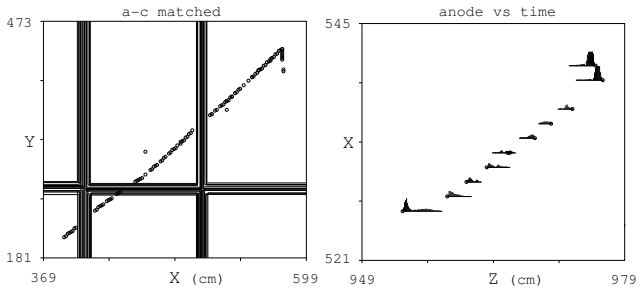

FIG. 21: An example event display from the Soudan detector, showing the long track from a muon and a shorter, more heavily ionizing track from a recoil proton.

through the holes relatively slowly, and does not produce the sharp pressure wave that caused the 2001 accident. The loss of light due to the extra water-acrylic interfaces is estimated to be a few percent and will be properly modelled in the detector simulation.

B. Fine Grained Tracking Detectors

The second major category of atmospheric neutrino detectors consists of comparatively fine resolution tracking detectors. The first generation of these experiments includes KGF [76], NUSEX [77], Frejus [78] and Soudan 1. The Soudan 1 detector was 30 tons of iron-loaded concrete instrumented with proportional tubes. The design, but not the site, was changed for the later Soudan 2 detector [62]. These first generation detectors were smaller than the water Cherenkov detectors, but in most cases became operational somewhat earlier. Tracking detectors have an advantage in sensitivity because they can detect low velocity charged particles that would be below Cherenkov threshold in water. In particular, the Soudan 2 detector is able to reconstruct the short and heavily ionizing trajectory of recoil protons from atmospheric neutrino events such as $\nu_\mu + n \rightarrow \mu^- + p$, as shown in Fig. 21. The complete specification of the two-body final state allows for the selection of low energy neutrino events with well-measured direction and energy, which is important to neutrino oscillation through the ratio L/E. The Soudan collaboration combines these quasi-elastic events with a higher energy sample including events with visible energy greater than 600 MeV and with multiple tracks in the final state. They estimate a pointing resolution of $20^\circ - 30^\circ$ and a $\log(L/E)$ resolution of 0.5. Analysis of this data, shown in Fig. 22 yields the confidence interval shown in Fig. 19.

Liquid argon TPCs such as the upcoming ICARUS experiment [79] will reconstruct event details including the ionization level of charged tracks with unprecedented resolution. The first generation detectors will be relatively small; the first installation of ICARUS at Gran Sasso will be 600 tons, with a planned increase to 3 ktons. There are ideas to build even larger liquid argon TPCs [80].

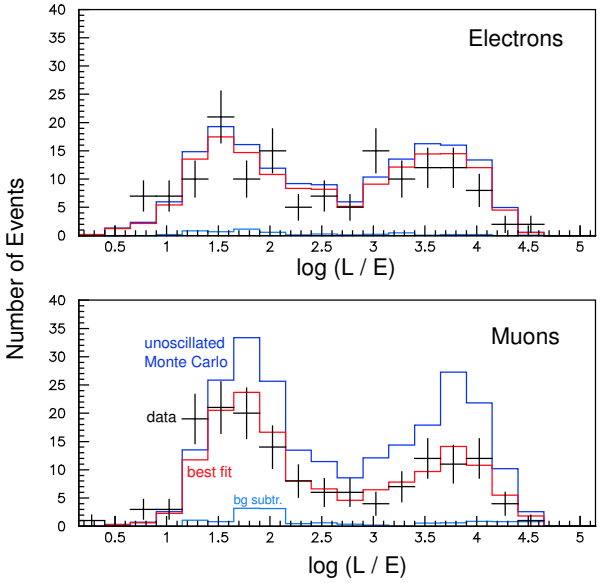

FIG. 22: The L/E distribution for high resolution atmospheric neutrinos in the Soudan 2 analysis.

No significant signal of proton decay was ever detected by any of the iron-based tracking experiments, however each did measure the background from atmospheric ν_μ and ν_e interactions. In the early history of the atmospheric neutrino anomaly, a dichotomy appeared where the water Cherenkov detectors Kamiokande [69] and IMB [70] measured a ν_μ/ν_e ratio inconsistent with expectation, whereas the non-water detectors NUSEX [81] and Frejus [82] did not, although with poorer event statistics. This is shown in Fig. 23, including data points from more recent experiments as well. The difference between water and iron detectors led to studies of neutrino interactions with light nuclei versus heavy nuclei, but resulting in no identification of a cause for the different results. Ultimately, the explanation is likely to be statistical, as the larger data set from Soudan 2 now clearly measures an anomalous ν_μ/ν_e ratio with the hallmarks of neutrino oscillation [83].

There is a second category of fine grained tracking detector that is mostly sensitive to muon neutrinos in the form of upward-going muons. These include the Baksan and MACRO experiments, which have fairly small absorber mass (a few hundred tons) and were never intended to detect proton decay. The MACRO detector, shown in Fig. 24, was composed of three horizontal planes of liquid scintillator tanks separated by several meters, with the lower section filled with crushed rock absorber and a hollow upper "attico" section. The sides of the detector are also covered with vertical planes of scintillator. Analysis of the upward through-going muon sample yields the confidence interval shown in Fig. 19. In addition to through-going muons, MACRO has analyzed partially contained and stopping topologies, where the crushed rock in the lower section acts as target or stop-

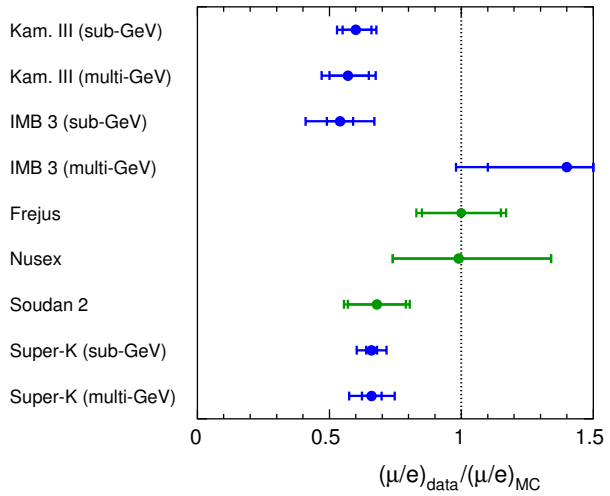

FIG. 23: A compendium of the measurements of the double ratio ν_μ/ν_e(data) to ν_μ/ν_e(M.C.) for atmospheric neutrino experiments.

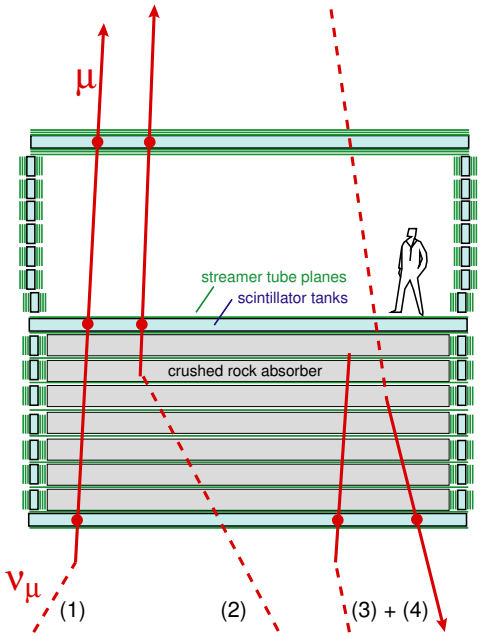

FIG. 24: An end view of the MACRO detector, showing different categories of neutrino-induced events: (1) upward through-going muon events, (2) upward partially-contained events, (3) upward stopping muon events, and (4) downward partially contained events.

ping absorber respectively [84].

Time-of-flight detectors identify the direction of the muon by measuring the time interval as the muon traverses two or more layers of liquid scintillator. Figure 25 shows the $1/\beta$ distribution for throughgoing upward muons reconstructed by the MACRO experiment, clearly separating several hundred neutrino induced events from the background of several million downward-going cosmic rays [85].

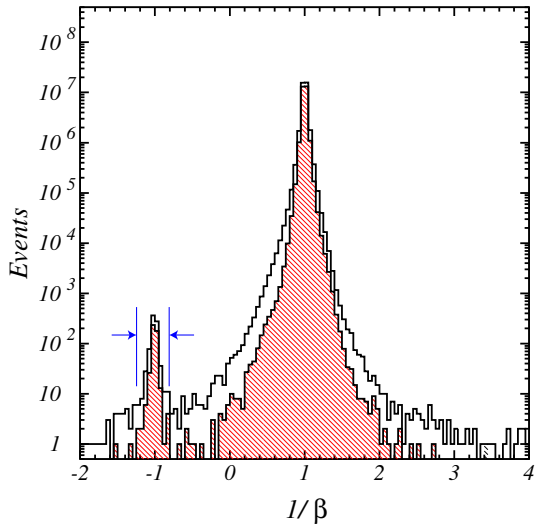

FIG. 25: Distribution of $1/\beta$ for all muons in the data. A clear peak of upward-going muons is evident. The shaded part of the distribution is for the subset of events where three scintillator layers were hit.

Fine-grained tracking also allows a crude muon energy estimate by measuring the amount of multiple coulomb scattering (MCS). One of several empirical formula [86] gives the r.m.s. lateral displacement of a relativistic muon after crossing absorber thickness X, measured in radiation lengths:

$$\sigma_{proj}^{MCS} \sim \frac{X}{\sqrt{3}} \frac{13.6MeV}{p_\mu \beta c} \sqrt{\frac{X}{X_0}} (1 + 0.038 \ln \frac{X}{X_0}). \quad (3)$$

For MACRO, $\sigma_{proj}^{MCS} \sim 10cm/E_\mu(GeV)$. Because the MACRO streamer tube tracking was designed to measure the transit of slow particles such as magnetic monopoles, the detector is equipped with timing electronics that records the streamer drift times. This allows a spatial resolution of $\sim$ 0.3 cm (in a 2.9 cm wide cell), verified by beam test studies. The technique saturates for muon energies above 40 GeV, below which the parent neutrino energy may be estimated with a resolution of $\delta E_\nu/E_\nu \sim 150\%$.

There is a final category of atmospheric neutrino detector that includes magnetic tracking. The first such detector, MINOS [87], was designed mostly for a long-baseline accelerator beam, and therefore has a built in orientation along the neutrino beam direction. MINOS will be composed of 486 layers of iron sandwiched with 4-cm wide by 1-cm thick strips of plastic scintillator, with a total mass of 5.4 ktons. The average magnetic field strength is 1.3 Tesla. MINOS can make a unique contribution to atmospheric neutrino studies by measuring the $\nu_\mu/\bar{\nu}_\mu$ ratio. This will test the near unity ratio predicted by atmospheric neutrino flux models, and possibly provide CPT tests of different oscillation probability for ν_μ and $\bar{\nu}_\mu$.

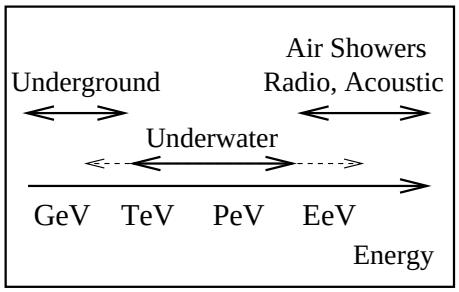

FIG. 26: Energy range of the various detection techniques (see below). Optical Cherenkov detectors, although optimized to the TeV-PeV range, are sensitive also at lower and higher energies, as indicated by the dashed lines.

In addition, the magnetic field of MINOS will allow for the momentum determination of exiting muons up to approximately 70 GeV. This will provide a sample of ν_μ interactions with relatively accurate L and E_ν determination for neutrino oscillation studies. This analysis was also proposed for a much larger underground neutrino detector called MONOLITH [88]. MONOLITH would use a very large mass of magnetized iron for the goal of measuring L/E with resolution sufficient to resolve the oscillatory pattern in atmospheric neutrino oscillations [88].

VI. HIGH ENERGY NEUTRINO TELESCOPES

Whereas MeV neutrino astronomy has been established by the observation of solar neutrinos and neutrinos from supernova SN1987A, neutrinos with energies of GeV to PeV (10^6 GeV), which must accompany the production of high energy cosmic rays, still await discovery. Detectors underground have turned out to be too small to detect the feeble fluxes of energetic neutrinos from cosmic accelerators. The high energy frontier of TeV (= 10^3 GeV) and PeV energy is currently being tackled by much larger, expandable arrays constructed in open water or ice. Detectors tailored to record acoustic, radio, fluorescence or air shower signatures from neutrino interactions at EeV energy (= 10^9 GeV) and above are being designed in parallel. Fig. 26 sketches the energy domains of different techniques.

A. Physics Goals

The central goal of high energy neutrino telescopes is to settle the origin of high energy cosmic rays [89]. The directional information of these charged particles - protons, light and heavy nuclei - is lost due to deflection in cosmic magnetic fields (apart from the extreme energies above 10^{10} GeV where deflection is negligible). Source tracing, i.e. *astronomy*, is only possible by neutral, stable particles like γ rays and neutrinos. In contrast to γ rays which may come from pure electron acceleration, only neutrinos provide incontrovertible evidence of proton acceleration. On top of that, neutrinos do not suffer from absorption by the omnipresent infrared or radio background when propagating through space. The range of TeV γ rays is only about 100 Mpc, at PeV only 10 kpc, i.e. about the radius of our Galaxy. Therefore, the topology of the far distant high energy Universe may possibly be investigated only with neutrinos.

The physics goals of high energy neutrino telescopes include:

a) Search for neutrinos from cosmic acceleration processes in galactic sources like micro quasars or supernova remnants (SNR), or extragalactic sources like active galactic nuclei (AGN) or gamma ray bursts (GRB),

b) search for ultra-high energy (UHE) neutrinos from interactions of UHE cosmic rays with the photons of the cosmic 3K microwave background (the so called GZK – Greisen-Zatsepin-Kuzmin – neutrinos), from topological defects (TD) or from the decay of super-heavy particles,

c) search for neutrinos from the annihilation of Weakly Interacting Massive Particles (WIMPs),

d) search for magnetic monopoles,

e) monitoring our Galaxy for MeV neutrinos from supernova bursts.

Most models related to sources of type *a)* assume acceleration by shock waves propagating in accretion discs around black holes or along the extended jets emitted perpendicularly to the disk (bottom-up models). Neutrinos are generated in decays of mesons produced by interactions of the accelerated charged particles with ambient matter or with photon gas.

$$p + p(\gamma) \rightarrow p(n) + \pi \qquad \searrow \mu + \nu$$

The neutrino energy spectrum of many models follows an E_ν^{-2} behaviour, at least over a certain range of energy. Assuming an E_ν^{-2} form and normalizing the neutrino flux to the measured flux of cosmic rays at highest energies leads to an upper bound of $dN/dE_\nu \sim 5 \times 10^{-8} E_\nu^{-2}$ GeV^{-1} cm^{-2} s^{-1} sr^{-1} to the diffuse neutrino flux (i.e. the flux integrated over all possible sources) [90]. Reasonably weakened assumptions loosen this bound by more than one order of magnitude to $10^{-6} E_\nu^{-2}$ GeV^{-1} cm^{-2} s^{-1} sr^{-1} [91](see also Fig.30). The so-called top-down scenarios of type *b)* are suggestive for the explanation of highest energy cosmic rays. In this scenario, high energy particles would be "born" with high energies, and not accelerated from low to high energies, as in the standard bottom-up scenarios.

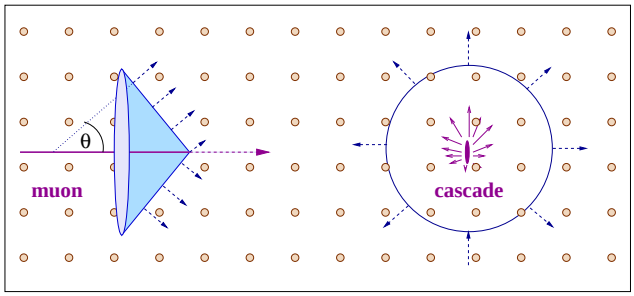

FIG. 27: Detection of muon tracks (left) and cascades (right).

We will focus on *a)* and *b)* in the following and refer to [89, 92, 93, 94] and references therein for more information on *c)* - *e)*.

B. Cherenkov telescopes under water and ice

Optical underwater/ice neutrino detectors consist of a lattice of photomultipliers (PMTs) housed in transparent pressure spheres which are spread over a large open volume in the ocean, in lakes or in ice. In most designs the spheres are attached to strings which - in the case of water detectors - are moored at the ground and held vertically by buoys. The typical spacing along a string is 10-20 meters, and between strings 30-100 meters. The spacing is very large compared to Super-Kamiokande. This allows large volumes to be covered but makes the detector practically blind with respect to phenomena below 10 GeV.

The PMTs record arrival time and amplitude of Cherenkov light emitted by muons or particle cascades. The accuracy in time is a few nanoseconds. Fig. 27 sketches the two basic detection modes.

In the *muon* mode, high energy neutrinos are inferred from the Cherenkov cone accompanying muons which enter the detector from below. Such upward moving muons can have been produced only in interactions of muon neutrinos having crossed the earth. The effective volume considerably exceeds the actual detector volume due to the large range of muons (about 1 km at 300 GeV and 24 km at 1 PeV). Muons which have been generated in the earth atmosphere above the detector and punch through the water or ice down to the detector, outnumber neutrino-induced upward moving muons by several orders of magnitude and have to be removed by careful up/down assignment. At energies above a few hundred TeV, where the earth is going to become opaque even to ν_e and ν_μ neutrinos, muons arrive only from directions close to the horizon, at EeV energies even only from the upper hemisphere. Most of these muons can be distinguished from down going atmospheric muons due to their higher energy deposition.

Apart from elongated tracks, *cascades* can be detected. Their length increases only like the logarithm of the cascade energy. With typically 5-10 meters length, and a diameter of the order of 10 cm, cascades may be considered as quasi point-like compared to the spacing of photomultipliers in Cherenkov telescopes. The effective volume for cascade detection is close to the geometrical volume. While for present telescopes it therefore is much smaller than that for muon detection, for kilometer-scale detectors and not too large energies it can reach the same order of magnitude as the latter.

Underwater/ice telescopes are optimized for the detection of muon tracks and for energies of a TeV or above, by the following reasons:

a) Above one TeV, the spectrum of atmospheric neutrinos changes from E^{-3} to $E^{-3.7}$ dependence. This is significantly steeper than the expected spectrum of neutrinos from cosmic accelerators and results in a much better signal-to-background ratio at higher energies.

b) Neutrino cross section and muon range increase with energy. The larger the muon range, the larger is the effective detection volume.

c) The mean angle between muon and neutrino decreases with energy like $E^{-0.5}$, with a pointing accuracy of about one degree at 1 TeV.

d) Mainly due to pair production and bremsstrahlung, the energy loss of muons increases with energy. For energies above 1 TeV, this allows an estimate of the muon energy from the larger light emission along the track.

The development in this field was stimulated originally by the DUMAND project close to Hawaii which was cancelled in 1995. The breakthrough came from the other pioneering experiment located at a depth of 1100 m in the Siberian Lake Baikal. The BAIKAL collaboration not only was the first to deploy three strings (as necessary for full spatial reconstruction [95]), but also reported the first atmospheric neutrinos detected underwater ([96], see Fig. 28, left). At present, NT-200 is taking data, an array comprising 192 mushroom shaped 15"-PMTs on 4 strings. A moderate upgrade (NT200+) is planned for 2004.

With respect to its size, NT-200 has been surpassed by the AMANDA detector [97]. Rather than water, AMANDA uses the 3 km thick ice layer at the geographical South Pole. Holes are drilled with hot water, and strings with PMTs are frozen into the ice. With 677 PMTs at 19 strings, most at depths between 1500-2000 m, the present AMANDA-II array reaches an area of a few 10^4 m^2 for 1 TeV muons. AMANDA-II may be the first detector with a realistic discovery potential with respect to extraterrestrial high energy neutrinos, even though it is smaller than the square kilometer size generally predicted to be required for clear observation of such signals. Limits obtained from the analysis of data taken with the smaller ten-string detector AMANDA-B10 in 1997 are similar to or below those limits which have been obtained by underground detectors over more

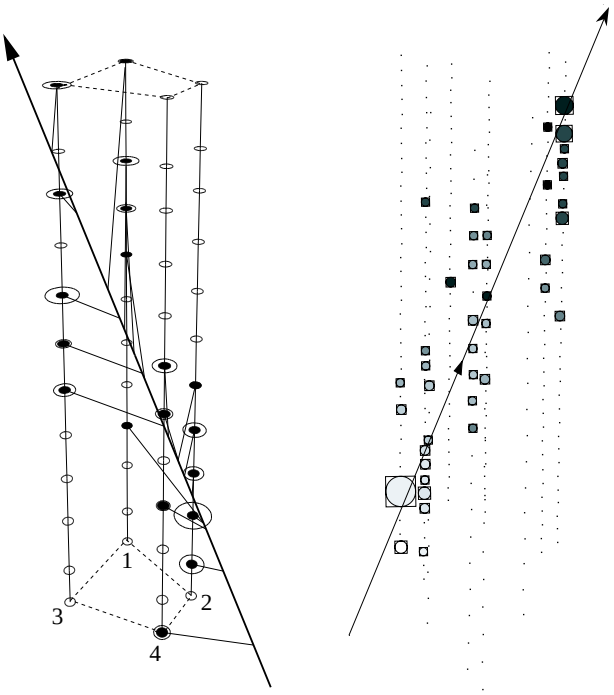

FIG. 28: Left: one of the first clearly upward moving muons recorded with the 1996 four-string-stage of the Baikal detector. Small ellipses denote PMTs. Hit PMTs are black, with the size of the disc proportional to the recorded amplitude. The arrow line represents the reconstructed muon track, the thin lines the photon paths. Right: Upward muon recorded by the 1997 version of AMANDA. Small dots denote the PMTs arranged on ten strings. Hit PMTs are highlighted by boxes, with the degree of shadowing indicating the time (dark being late), and the size of the symbols the measured amplitude. Note the different scales: the height of the Baikal array is 72 meters, that of AMANDA nearly 500 meters.

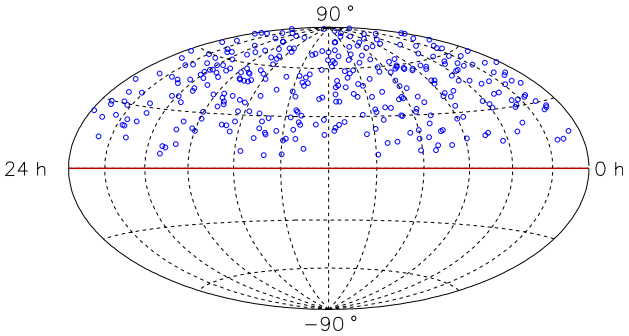

FIG. 29: Sky map of 300 neutrino candidates taken with AMANDA B10 in 1997. No indication of extraterrestrial point sources on top of atmospheric neutrinos are found.

than a decade of data taking. The limit [99] on the diffuse flux from unresolved sources with an assumed E^{-2} spectrum is $0.8 \cdot 10^{-6} E_\nu^{-2}$ GeV^{-1} cm^{-2} s^{-1} sr^{-1}, slightly below the loosest theoretical bounds [91] and a factor of 2 below the corresponding Baikal limit. AMANDA limits on point sources on the Northern sky [101] complement the limits obtained from detectors in the Northern hemisphere for the Southern sky (see Fig. 31). The overall sensitivity of AMANDA-B10 has been verified by samples of events which are dominated by atmospheric neutrinos [98]. Fig. 28 (right) shows an neutrino event taken with AMANDA-B10, Fig. 29 shows the sky map of the first 300 neutrino candidates taken in 1997.

Based on the experience from AMANDA, a cubic kilometer detector, ICECUBE [102], is going to be deployed at the South Pole. It will consist of 4800 PMTs on 80 vertical strings, with 125 m inter-string-distances and a 16 m spacing between the PMTs along a string. The 8-inch AMANDA PMTs will be replaced by 10-inch PMTs, and the simple analog-readout by a digital readout of the full transient waveform recorded by the PMT.

Two projects for large neutrino telescopes are under construction in the Mediterranean - ANTARES [103] and NESTOR [104] . Both have assessed the relevant physical and optical parameters of their sites and have deployed prototype arrays of about a dozen PMTs. ANTARES and NESTOR follow different deployment schemes and array designs. The NESTOR group plans to deploy a tower of several floors, each carrying 12 PMTs at 16 m long arms. The ANTARES detector will consist of 12 strings, each equipped with 30 triplets of PMTs. This detector will have an area of about $2 \cdot 10^4$ m^2 for 1 TeV muons - similar to AMANDA-II - and is planned to be fully deployed in 2006. An additional initiative, NEMO, has finished a series of site explorations at a location 70 km from Sicily and is now in the phase of prototype studies for a cubic kilometer detector [105]. The different efforts are going to converge towards one single project for a cubic kilometer detector.

There have been longstanding discussions about the best location for a future large neutrino telescope. One detector in each hemisphere will be necessary for full sky coverage. With respect to optical properties, water detectors in oceans seem to be favoured: although the absorption length of Antarctic ice at Amanda depths is more than 1.5 times that in oceans (and about four times that of Baikal), ice is characterized by strong light scattering, and its optical parameters vary with depth. Light scattering leads to a considerable delay of Cherenkov photons. On the other hand ice does not suffer from the high potassium content of ocean water or from bioluminescence. These external light sources result in counting rates ranging from several tens of kHz to a few hundred kHz per PMT, compared to less than 500 Hz per PMT dark count rate in ice. Depth arguments favour oceans. Note, however, that this argument lost some of its initial strength after BAIKAL and AMANDA developed reconstruction methods which effectively reject even the high background at shallow depths. What counts most, at the end, are basic technical questions like deployment, or the reliability of the single components as well as of the whole system. Systems with a non-hierarchical structure like AMANDA (where each PMT has its own 2 km cable to surface) will suffer less from single point failures than

water detectors do. In the case of water, longer distances between the detector and the shore station have to be bridged. Consequently, not every PMT can get its own cable to shore, resulting in a hierarchical system architecture. This drawback of water detectors may be balanced by the fact that they allow retrieval and replacements of failed components, as the BAIKAL group has demonstrated over many years.

C. Acoustic detection

A high energy particle cascade deposits energy into the medium via ionization losses, which is immediately converted into heat. The effect is a fast expansion, generating a bipolar acoustic pulse. Transverse to the pencil-like cascade (diameter about 10 cm) the radiation propagates within a disk of about 10 m thickness (the length of the cascade) into the medium. The signal power peaks at 20 kHz where the attenuation length of sea water is a few kilometers, compared to a few tens of meters for light. Given a large initial signal, huge detection volumes can be achieved. With efficient noise rejection, acoustic detection might be competitive with optical detection at multi-PeV energies [106] .

Present initiatives [94] envisage combinations of acoustic arrays with optical Cherenkov detectors (NESTOR, ANTARES, ICECUBE) or the use of existing sonar arrays for submarine detection close to Kamchatka and in the Black Sea [107]. Most advanced is AUTEC, a project using a very large hydrophone array of the US Navy, close to the Bahamas [108] . The existing array of 52 hydrophones spans an area of 250 km^2 and has good sensitivity between 1-50 kHz. Due to the sparse instrumentation, it is expected to trigger only on events above 100 EeV.

D. Radio detection

Electromagnetic showers generated by high energy electron neutrino interactions emit coherent Cherenkov radiation. Electrons are swept into the developing shower, which acquires a negative net charge from the added shell electrons. This charge propagates like a relativistic pancake of 1 cm thickness and 10 cm diameter. Each particle emits Cherenkov radiation, with the total signal being the resultant of the overlapping Cherenkov cones. For wavelengths larger than the cascade diameter, coherence is observed and the signal rises proportional to E^2, making the method attractive for high energy cascades. The bipolar radio pulse has a width of 1-2 ns. In ice as well as in salt domes, attenuation lengths of several kilometers can be obtained, depending on the frequency band, the temperature of the ice, and the salt quality. Thus, for energies above a few tens of PeV, radio detection in ice or salt might be competitive or superior to optical detection.

A prototype Cherenkov radio detector called RICE is operating at the geographical South Pole [110]. Twenty receivers and emitters are buried at depths between 120 and 300 m. From the non-observation of very large pulses, a limit of about $10^{-5}E_\nu^{-2}$ GeV^{-1} cm^{-2} s^{-1} sr^{-1} has been derived for energies above 100 PeV [100]. SALSA, a R&D project study for radio detection in natural salt domes, promises to get a limit about three orders of magnitude better [111] . ANITA (ANtarctic Impulsive Transient Array) is an array of radio antennas planned to be flown at a balloon on an Antarctic circumpolar path in 2006 [112]. From 35 km altitude it may record the radio pulses from neutrino interactions in the thick ice cover and monitor a really huge volume. The expected sensitivity from a 30 day flight is about $10^{-7}E_\nu^{-2}$ GeV^{-1} cm^{-2} s^{-1} sr^{-1} at 10 EeV.

Most exotic is the Goldstone Lunar Ultrahigh Energy Neutrino Experiment, GLUE. It has searched for radio emission from extremely-high energy cascades induced by neutrinos or cosmic rays skimming the moon surface [113]. Using two NASA antennas, an upper limit of $5 \cdot 10^{-5}E_\nu^{-2}$ GeV^{-1} cm^{-2} s^{-1} sr^{-1} at 100 EeV has been obtained.

E. Detection of neutrino energies via air showers

At supra-EeV energies, large extensive air shower arrays like the AUGER detector in Argentina [114] or the telescope array [115] may search for horizontal air showers due to neutrino interactions deep in the atmosphere (showers induced by charged cosmic rays start on top of the atmosphere). AUGER consists of an array of water tanks that will span an area of more than 3000 km^2 and will record the Cherenkov light of air-shower particles crossing the tanks. It is combined with telescopes looking for the atmospheric fluorescence light from air showers. The optimum sensitivity window for this method is at 1-100 EeV, the effective detector mass is between 1 and 20 Giga-tons, and the estimated sensitivity is of the order of $10^{-7}E_\nu^{-2}$ GeV^{-1} cm^{-2} s^{-1} sr^{-1}. An even better sensitivity might be obtained for tau neutrinos, ν_τ, scratching the Earth and interacting close to the array. The charged τ lepton produced in the interaction can escape the rock around the array, in contrast to electrons, and in contrast to muons it decays after a short path into hadrons [116]. If this decay happens above the array or in the field of view of the fluorescence telescopes, the decay cascade can be recorded. Provided the experimental pattern allows clear identification, the acceptance for this kind of signals can be large. For the optimal energy scale of 1 EeV, the sensitivity might reach $10^{-8}E_\nu^{-2}$ GeV^{-1} cm^{-2} s^{-1} sr^{-1}. A variation of this idea is to search for tau lepton cascades which are produced by horizontal PeV neutrinos hitting a mountain and then decay in a valley between target mountain and an "observer" mountain [117].

Already in the middle of 1990's, the Fly's Eye collaboration [118], and more recently, the Japanese AGASA

collaboration [119] have practiced the search mode of horizontal air showers. AGASA derived an upper limit of the order of 10^{-5} in the units given above - only just one order of magnitude above some predictions for AGN jets and for topological defects.

Heading to higher energies leads to space based detectors monitoring larger volumes than visible from any point on the Earth surface. The projects EUSO [120] and OWL [121] intend to launch large aperture optical detectors to 500 km height. The detectors would look down upon the atmosphere and search for nitrogen fluorescence signals due to neutrino interactions. The monitored mass would be up to 10 Tera-tons, with an energy threshold of about 10^{10} GeV.

F. Scenario for the next decade

The next ten years promise to be a particularly exciting decade for high energy neutrino astrophysics. Figures 30 and 31 sketch possible scenarios to move the frontier towards unprecedented sensitivities.

Figure 30 addresses the sensitivity to diffuse fluxes, i.e. integrating over the full angular acceptance of the detectors. The scale is set by the known flux of atmospheric neutrinos, by the bounds derived from observed fluxes of charged cosmic rays (W&B [90] and, with less stringent assumptions, the lower MPR curve [91]), by gamma rays (horizontal MPR line which assumes that cosmic rays are mostly confined in the cosmic source region and only gammas and neutrinos escape), and by specific model predictions [124]. The figure shows two of the latter, one for the predicted flux of GZK neutrinos at ultra-high energies (see item *b)* above), the other for a model of neutrinos from Active Galactic Nuclei, peaking at TeV-PeV energies (Stecker and Salomon, SS [122]). The majority of the limits shown are published as "differential" limits, defining the flux sensitivity as the neutrino flux which gives at least one observed event per decade of energy per year (assuming negligible background). The limits published for AMANDA assume an E^{-2} flux. They come from two separate analyses, the one studying upward muon tracks, the other downward tracks of very high energy which are unlikely to be due to muons generated in the atmosphere. Both analyses, however, properly account for the background of these atmospheric muons. The lines marked *1* and *2* extend over the energy range containing 90% of the events expected from an E^{-2} flux. For better illustration of the progress in time and over all the energy range, the AMANDA limits as well as the limits expected for ICECUBE have been translated to limits differentially per energy decade.

The present frontier is defined by TeV-PeV limits obtained by AMANDA and BAIKAL, and by PeV-EeV limits from the South Pole radio array RICE and the Japanese AGASA air shower array. Note that the Baikal/Amanda limits just reached a level sufficient to test (and actually to exclude) the model shown. The

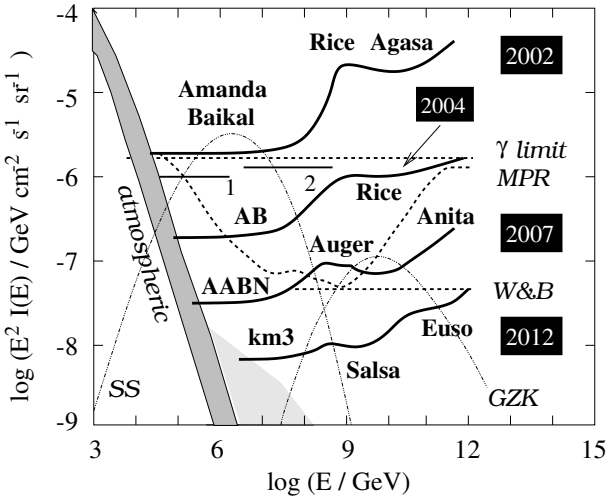

FIG. 30: Scenario for the improvement of experimental sensitivities to diffuse extraterrestrial fluxes of high energy neutrinos. AB = Amanda, Baikal, AABN = Amanda, Antares, Baikal, Nestor. *1,2,:* Amanda limits obtained from the analysis of upward (1) and high energy downward (2) tracks, assuming an E^{-2} spectrum. The grey band denotes the flux of atmospheric neutrinos, with the excess at high energies being an estimate for the contribution from prompt muons and neutrinos due to charm decays in air showers. Dashed lines indicate various theoretical bounds, the 2 thin curves specific flux predictions (see text).

progress over the next 2 years will come from the same experiments. After that, the Mediterranean telescopes – ANTARES and NESTOR – will start to contribute, flanked by AUGER and the ANITA balloon mission at high energies. This could result in an improvement of about two orders of magnitude over the full relevant energy range. Finally, ten years from now, the TeV-PeV sensitivity will be dictated by the cubic kilometer arrays at the South Pole and in the Mediterranean (marked as "km3"). At the high energy frontier, a SALSA-like experiment, and still higher, satellite detectors, might push the limit down by about three orders of magnitude compared to 2002.

Most likely, the first signal with clear signature will be a point source, possibly a transient signal which is easiest to identify. Figure 31 sketches a possible road until 2012. Best present limits are from MACRO, Super-Kamiokande (Southern sky) and AMANDA (Northern sky). This picture will not change until the Mediterranean detectors come into operation. AMANDA and ANTARES/NESTOR have the first realistic chance to discover an extraterrestrial neutrino source. The ultimate sensitivity for the TeV-PeV range is likely reached by the cubic kilometer arrays. This scale is set by many model predictions for neutrinos from cosmic accelerators or from dark matter decay. However, irrespective of any specific model prediction, these gigantic detectors, hundred times larger than AMANDA and thousand times larger than underground detectors, will hopefully keep

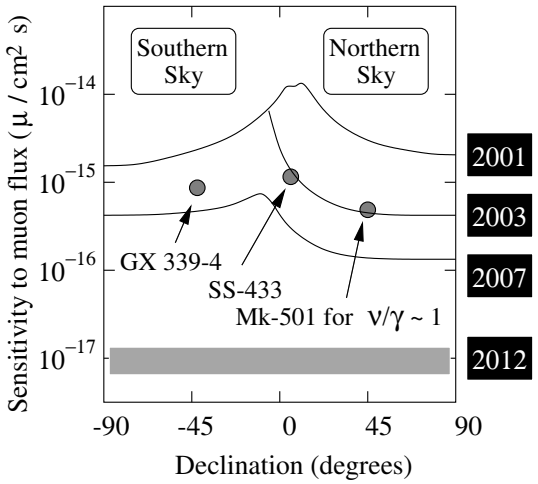

FIG. 31: Scenario for the improvement of experimental sensitivities to TeV point sources. Expected steps for the Northern sky are obtained from Amanda (2003), and Amanda together with the first strings of IceCube (2007), on the Southern sky from the Mediterranean detectors Antares and Nestor (2007). In 2012, both hemispheres will have profited from cubic kilometer arrays indicated by the grey band. Shown are also predicted fluxes for two microquasars [123] - one in the northern and one in the southern hemisphere - which are just in reach for Amanda and the Mediterranean arrays. As a benchmark, we show also the flux which would be expected if Mk501, a source spectacular in TeV gamma rays, would produce a similar flux in TeV neutrinos.

the promise for any detector opening a new window to the Universe: to detect *unexpected* phenomena.

[1] Davis et al., *Phys. Rev. Lett.* **14** (1968) 20; B.T. Cleveland, T. Daily, R. Davis, Jr., J.R. Distel, K. Lande, C.K. Lee, P.S. Wildenhain, J. Ullman, *Astrophys. J.***496** (1998) 505.

[2] K. Hagiwara et al. *Phys. Rev.***D 66** (2002) 010001.

[3] Z. Maki, N. Nakagawa and S. Sakata, *Prog. Theor. Phys* **28** (1962) 870, B. Pontecorvo *J. Expt. Theoret. Phys***33** (1957) 549 *J. Expt. Theoret. Phys***34** (1958) 247, V. Gribov and B. Pontecorvo *Phys. Lett.***B28** (1969) 493.

[4] S. P. Mikheyev and A. Y. Smirnov, in Massive Neutrinos in Astrophysics and in Particle Physics, Proceedings of the Moriond Workshop, edited by O. Fackler and J. Tran Thanh Van, Editions Frontières, Gif-sur-Yvette, 335 (1986); S.P.Mikheyev and A.Yu. Smirnov, *Sov. J. Nucl. Phys.* **42** (1985) 1441; L. Wolfenstein, *Phys. Rev.* **D 17** (1978) 2369.

[5] Q.R. Ahmad et al. *Phys. Rev. Lett.***89** (2002) 011301

[6] S. Fukuda et al. *Phys. Rev. Lett.***86** (2001) 5651; S. Fukuda *et al.*, *Phys. Lett. B* **539** (2002) 179; M.Smy, for the Super-Kamiokande collaboration, *Nucl. Phys. B (Proc. Suppl.)* 118 (2003) 25.

[7] J.N. Bahcall, M. H. Pinsonneault, and S. Basu, *Astrophys. J.* **555** (2001) 990.

[8] A.S. Brun, S. Turck-Chièze, and J.P. Zahn, *Astrophys. J.* **525**, 1032 (1999); S. Turck-Chièze *et al.*, *Ap. J. Lett.*, v. **555** July 1, 2001.

[9] V.N. Gavrin et al. *Nucl. Phys. B (Proc. Suppl.)***118** (2003) 39.

[10] W. Hampel et al. *Phys. Lett.* **B 447** (1999) 127 ; T. Kirsten *Proceedings of the Neutrino 2002 Conference, Munich* (2002)

[11] P. Anselmann et al. *Phys. Lett.* **B 342** (1995) 440; J.N. Abdurashitov et al. *Phys. Rev. Lett.* **77** (1996) 4708; W. Hampel et al. *Phys. Lett.* **B 420** (1998) 114

[12] Y. Fukuda et al. *Phys. Rev.***D 44** (1996) 1683.

[13] E. Eguchi et al. *Phys. Rev. Lett.* **90** (2003) 021802.

[14] A. J. Baltz and J. Weneser, *Phys. Rev. D* **37** (1988) 3364; M. C. Gonzalez-Garcia, C. Peña-Garay and A. Y. Smirnov *Phys. Rev. D***63** (2001) 113004.

[15] J. Boger et al. *Nucl. Inst. Meth.***A449** (2000) 72.

[16] Q.R. Ahmad et al. *Phys. Rev. Lett.***87** (2001) 071301.

[17] Q.R. Ahmad et al. *Phys. Rev. Lett.***89** (2002) 011302

[18] S. N. Ahmed et al. , nucl-ex/0309004.

[19] G.L. Fogli, E. Lisi, A. Marrone, D. Montanino, A. Palazzo, *Phys. Rev.***D66** (2002) 053010.

[20] J.N. Bahcall, *Phys. Rev.* **C 56** (1997) 3391.

[21] G.L. Fogli et al., hep-ph/0112127; M. Maltoni, T Schwetz and J.W.F. Valle, hep-ph/012129; J.N. Bahcall, M.C. Gonzales-Garcia and C. Penya-Garay, hep-ph/0212147; H. Nunokawa et al., hep-ph/0212202; P. Aliani et al., hep-ph/0212212; P.C. de Holanda and A.Yu. Smirnov, hep-ph/0212270.

[22] W. Hampel, priv. communication.

[23] John N. Bahcall, M. C. Gonzalez-Garcia, Carlos Pena-Garay, hep-ph/0204314

[24] T. Hagner *et al.*, *Astropart. Phys.* **14** (2000)33

[25] Borexino collaboration, G. Alimonti *et al.*, *Astropart. Phys.* **16** (2002) 205.
[26] Borexino collaboration, C. Arpesella *et al. Astropart. Phys.* **18** (2002) 1.
[27] Borexino collaboration, G. Alimonti *et al.*, *Astropart. Phys.* **8** (1998) 141; Borexino collaboration, G. Alimonti *et al.*, *Nucl. Instrum. Meth.* **A406** (1998) 411.
[28] A. Suzuki, 8th international workshop on neutrino telescopes, Venice, Feb. 23-26 1999; J. Busenitz *et al.,* "Proposal for US Participation in KamLAND, " March 1999 (unpublished), `http://kamland.lbl.gov/`.
[29] K. Inoue, First Sendai Int. Conf. on Neutrino Science, March 14-16, Sendai, Japan, `http://www.awa.tohoku.ac.jp/conf2002/program.html`.
[30] Borexino Collaboration, G. Alimonti *et al.*, *Phys. Lett.* **B 422** (1998) 349.
[31] LowNu 2002 workshop, Heidelberg, 2002, `http://www.mpi-hd.mpg.de/nubis/www_lownu2002/`.
[32] S. Schönert, *Nucl. Phys. B (Proc. Suppl.)* **110** (2002) 277.
[33] R.S. Raghavan,Phys. Rev. Lett. 7819973618; LENS collaboration, Letter of Intent, Laboratori Nazionali del Gran Sasso (1999); `http://www.mpi-hd.mpg.de/nubis/www_lownu2002/`
[34] H. Ejiri et al., *Phys. Rev. Lett.* **85** (2000) 2917.
[35] Y. Suzuki, LowNu2 workshop, Tokyo, 2000, `http://www-sk.icrr.u-tokyo.ac.jp/neutlowe/`,
[36] B. Lanou, LowNu 2002 workshop, Heidelberg, 2002, `http://www.mpi-hd.mpg.de/nubis/www_lownu2002/`.
[37] D.N. McKinsey and J.M. Doyle, *J. of Low Temp. Phys.* **118** (2000) 153.
[38] G. Bonvicini et al., Contributed paper, Snowmass 2001, hep-ex/0109199, hep-ex/0109032
[39] A. Burrows, D. Klein, R, Gandhi *Phys. Rev.***45** (1992) 3361
[40] V. Trimble; *Rev. Mod. Phys.* **60** (1988) 859-871.
[41] K. Hirata et al; *Phys. Rev. Lett.* **58** (1987) 1490-1493.
[42] R.M. Bionta et al; *Phys. Rev. Lett.* **58** (1987) 1494-1496.
[43] E.N. Alexeyev et al; JETP Lett. **45** (1987) 589.
[44] H.V. Klapdor-Kleingrothaus and K. Zuber; *Particle Astrophysics*, Institute of Physics, Bristol, 1997 and references therein.
[45] J. Heise, Ph.D. thesis, University of British Columbia (2002).
[46] E.D. Zimmerman, Proceedings of Workshop on Tau Lepton Physics, (TAU02), hep-ex/0211039.
[47] K. Scholberg, *in the Proceedings of Neutrino 2000 - the XIX International Conference on Neutrino Physics and Astrophysics, Sudbury, June 2000*, hep-ex/0008044.
[48] P. Vogel and J.F. Beacom; *Phys. Rev.* **D60** (1999) 53003-53012.
[49] J.F. Beacom, R.N. Boyd, and A. Mezzacappa; Phys. Rev. Lett. **85** (2000) 3568-3571 and astro-ph/0010398.
[50] A. Burrows; *Nature* **403** (2000) 727-733.
[51] S. Ando, K. Sato and T. Totani, *Astropart. Phys.* **18**, 307 (2003); M. Kaplinghat, G. Steigman, and T.P. Walker, *Phys. Rev.* **D62**, 043001 (2000); D.H. Hartmann and S.E. Woolsey, *Astropart. Phys.* **7**, 137 (1997); T. Totani, K. Sato, and Y. Yoshii, *Astrophys. J.* **460**, 303 (1996); T. Totani and K. Sato, *Astropart. Phys.* **3**, 367 (1995).
[52] M. Malek *et al.*, *Phys. Rev. Lett.* **90**, 061101 (2003).
[53] J.C. Pati and A. Salam, *Phy. Rev. Lett.* **31** 661 (1973).
[54] H. Georgi and S.L. Glashow, *Phy. Rev. Lett.* **32** 438 (1974).
[55] C. Berger *et al.*, *Nucl. Instrum. Meth.* **A262** 463 (1987).
[56] E.N. Alekseev *et al.*, *Phys. Part. Nucl.* **29** 254 (1998).
[57] K. Nakamura *et al.*, "Kamiokande", *in Physics and Astrophysics of Neutrinos, eds. M. Fukugita and A. Suzuki*, Springer-Verlag, 1994, p249.
[58] R. Becker-Szendy *et al.*, *Nucl. Instrum. Meth.* **A324** 363 (1993).
[59] M. Ambrosio, *et al.*, *Astrophys. J.* **546** 1038 (2001); M.M. Boliev, *et al. Proc. 24th Intl. Cosmic Ray Conf.(Rome)* 1, 722 (1995); R. Svoboda, *et al. Astrophys. J.* **315** 420 (1987).
[60] S. Fukuda, *et al.*, *Astrophys. J.* **578** 317 (2002).; M. Ambrosio, *et al.*, *Astrophys. J.* **546** 1038 (2001); R. Becker-Szendy, *et al. Astrophys. J.* **444** 415 (1995).
[61] M. Ambrosio, *et al.*, *Phys. Rev.* **D60** 082002 (1999); A. Habig, *et al. Proc. 27th Intl. Cosmic Ray Conf.(Hamburg)* hep-ex/0106024; J.M. LoSecco, *et al. Phys. Lett.* **B188** 388 (1987).
[62] W.W.M. Allison *et al.*, *Nucl. Instrum. Meth.* **A376** 36 (1996); *ibid. Nucl. Instrum. Meth.* **A381** 385 (1996).
[63] S.P. Ahlen *et al.*, *Nucl. Instrum. Meth.* **A324** 337 (1993); M. Ambrosio *et al.*, *Nucl. Instrum. Meth.* **A486** 663 (2002).
[64] Y. Fukuda *et al.*, *Phys. Lett.* **B433** 9 (1998); technical article in preparation.
[65] Y. Fukuda *et al.*, *Phys. Lett. B* **388** 397 (1996).
[66] W.W.M. Allison *et al.*, *Phys. Lett.* **B391** 491 (1997)
[67] C.Waltham, for the SNO collaboration, Proc. of the ICRC2001, Hamburg, Aug.2001, p.991.
[68] R. Claus *et al.*, *Nucl. Instrum. Meth.* **A261** 540 (1987).
[69] K.S. Hirata *et al.*, *Phys. Lett.* **B280** 146 (1992); see also [71].
[70] R. Becker-Szendy *et al.*, *Phys. Rev.* **D46** 3720 (1992).
[71] Y. Fukuda *et al.*, *Phys. Lett. B* **335** 237 (1994).
[72] Y. Fukuda *et al.*, *Phys. Rev. Lett.* **81** 1562 (1998).
[73] S. Fukuda *et al.*, *Phys. Rev. Lett.* **85** 3999 (2000).
[74] S. Raby, hep-ph/0211024.
[75] M. Apollonio *et al.*, *Phys. Lett.* **B466** 415 (1999).
[76] M.R. Krishnaswamy *et al.*, *Phys. Lett.* **106B** 339 (1981).
[77] G. Battistoni *et al.*, *Nucl. Instrum. Meth.* **A245** 277 (1986).
[78] Ch. Berger *et al.*, *Nucl. Instrum. Meth.* **A262** 463 (1987).
[79] ICARUS collaboration (F. Arneodo *et al.*), hep-ph/0103008.
[80] D.B. Cline, *et al.*, astro-ph/0105442.
[81] M. Aglietta *et al.*, *Europhys. Lett.* **8** 611 (1989).
[82] K. Daum *et al.*, *Z. Phys.* **C66** 417 (1995).
[83] W.W.M. Allison *et al.*, *Phys. Lett.* **B449** 137 (1999).
[84] M. Ambrosio *et al.*, *Phys. Lett.* **B478** 5 (2000).
[85] M. Ambrosio *et al.*, *Phys. Lett.* **B434** 451 (1998).
[86] K. Hagiwara *et al.*, *Phys. Rev.* **D66** 010001 (2002).
[87] S.G. Wojcicki, *Nucl. Phys. B (Proc. Suppl.)* **91** (2001) 216.
[88] T. Tabarelli de Fatis (for the MONOLITH collaboration), *Nucl. Phys.* **B110** (Proc. Suppl.) 352(2002).
[89] J.G. Learned, K. Mannheim, *Ann.Rev.Nucl.Phys.* **50** (2000) 679.
[90] E. Waxman, J. Bahcall, *Phys.Rev.* **D59** (1999) 023002.
[91] K. Mannheim, R. Protheroe, J. Rachen, *Phys.Rev.* **D63** (2001), astro-ph/9812398.
[92] T.K. Gaisser, F. Halzen, T. Stanev, *Phys. Rep.* **258**

(1995) 173.
[93] C. Spiering, *Nucl.Phys.Proc.Supp.* **91** (2000) 331 and astro-ph/0012532.
[94] C. Spiering, *Prog. in Part. and Nucl. Phys.*,**48** (2002) 43.
[95] I.A.Belolaptikov et al., *Astropart.Phys.* **7** (1997) 263.
[96] R.V.Balkanov et al., *Astropart.Phys.* **14** (2000) 61.
[97] E. Andres et al., *Astropart.Phys.* **13** (2000) 1.
[98] E. Andres et al., *Nature* **410** (2001) 441; J.Ahrens et al., *Phys.Rev.* **D66** (2002) 012005 and astro-ph/0205109.
[99] J. Ahrens et al., to appear in *Physical Review Letters*, astro-ph/0303218
[100] I. Kravchenko et al., astro-ph/0306408.
[101] J.Ahrens et al., *Astrophys.J.* **583** (2003) 1040 and astro-ph/0208006.
[102] A. Goldschmidt et al., *Proc. 27th ICRC* (2001) 1237 and C.Spiering et al., ibid. 1242.
[103] T. Montaruli et al., hep-ex/0201009.
[104] P. Grieder et al., *Nucl.Phys. B (Proc.Suppl.)* **97** (2001) 105.
[105] T. Montaruli et al., hep-ex/9905019.
[106] see e.g. J.G. Learned, *Phys.Rev.* **D1**, 19 (1979) 3293.
[107] A. Capone et al., *Proc. 27th ICRC* (2001) 2164.
[108] N. Lehtinen et al., astro-ph/010433.
[109] D. Saltzberg et al., *Phys.Rev.Lett.* **86** (2001) 2802.
[110] D. Seckel et al., astro-ph/0103300.
[111] P. Gorham et al.,*Nucl.Instr. and Meth.* **A490** (2002) 476 and hep-ex/0108027.
[112] P. Gorham et al., *Astrophys.J.* **575**, (2002) 378.
[113] P. Gorham et al., *Phys.Rev.* **D66**, (2002) 063004.
[114] A. Letessier-Selvon et al., *Proc. 27th ICRC* (2001) 1204.
[115] M.Sasaki and M.Jobashi, astro-ph/0204167.
[116] D. Fargion, *Proc. EPS Int. Conf. on High En. Phys., Budapest* (2001) JHEP PrHEP-hep2001/208, and hep-ph/0111289
[117] G.W.S.Hou and M.A.Huang, astro-ph/0204145.
[118] R.Baltrusaitis et al., *Phys.Rev.* **D31**, 2192 (1985).
[119] S. Yoshida et al., *Proc. 27th ICRC* (2001) 1142.
[120] L. Scarsi et al., *Proc.Int.Workshop on Neutrino Telescopes, Venice 2001*, **vol. II**, 545.
[121] D.B.Cline and F.W.Stecker, astro-ph/0003459.
[122] F.W.Stecker and M.H.Salomon, *Space Sci.Rev.* **75** (1996) 341.
[123] C. DiStefano, D. Guetta, A. Levinson, E. Waxmann, *Astrophys.J.* **575** (2002) 378, and astro-ph/0202200.
[124] see for a recent discussion of bounds and models O.Kalashev, V.Kuzmin, D.Semikoz and G.Sigl, *Phys.Rev.* **D66** (2002) 063004 and hep-ph/0205050.